7-23-2020

Programmable Self-Assembly of Biomolecules Triggered by the Active Nematic Disclinations Network

Kamal Bahadur Ranabhat

PROGRAMMABLE SELF-ASSEMBLY OF BIOMOLECULES TRIGGERED BY THE ACTIVE NEMATIC DISCLINATIONS NETWORK

by

Kamal B. Ranabhat

A Thesis

Submitted in Partial Fulfillment of

the Requirements for the Degree of

Master of Science

Major: Physics & Materials Science

The University of Memphis

August 2020

ACKNOWLEDGMENTS

I would like to express my sincere gratitude to my supervisor, Dr. Chenhui Peng, for the continuous support of my work. As an advisor, he has taught me more than I could ever learn in this scientific exploration. He has shown me many times that one needs to be very diligent along with the smart ways for any project to take in right directions. Not only in terms of profession, he is very good in personal matter as well and I believe I was able to copy at least some of his good virtues. I am always grateful to his honest reviews, comments and criticisms that led me complete the project with genuine effort.

I am sincerely thankful to Dr. Firouzeh Sabri and Dr. Jahan for accepting my request to join my thesis committee. Each of the members of my Dissertation Committee has provided me extensive professional guidance and taught me a great deal about scientific research. Also, I am grateful to all of those with whom I have had the pleasure to work during this project. I am equally thankful to all other faculty members and staff of the Department of Physics and Materials Science, University of Memphis.

I would like to thank my family for supporting me throughout the entire process even being so far from me. They have always inspired me to work hard and led me envision my career in this scientific journey. Last but not the least, I would like to express my gratitude to my friends and all those with whom I have had the pleasure to work during this project.

Kamal B. Ranabhat

June 16, 2020

Memphis, TN, USA

Table of Contents

List of figures

List of Abbreviations:

LC	Liquid Crystal
POM	Polarizing Optical Microscope
SD1	Azo dye
RM257	2-Methyl-1,4-phenylene bis (4-(3-(acryloyloxy) propoxy) benzoate
CCD	Charged Coupled Device
LOI	Lines of Interest
DMF	N-N Dimethylformamide
UV	Ultraviolet
SEM	Scanning Electron Microscopy
nm	nanometer
µm	micrometer
BODIPY C-5	4,4-Difluoro-5,7-Dimethyl-4-Bora-3a,4a-Diaza-s-Indacene-3-Pentanoic Acid
5 CB	4-Cyano-4'-pentylbiphenyl

List of Symbols:

n	Director field
S	Order parameter
D	Dimension
n_e	Refractive index of extraordinary ray
n_o	Refractive index of ordinary ray
I_0	Intensity of incident light
I	Intensity of light
P	Polarizer
A	Analyzer
φ	Rotation angle
m	Topological charge
R_1	Rotational speed of the polarizer
R_2	Rotational speed of the projection of light

Chapter 1. Introduction

1.1 Introduction to Liquid Crystals

Liquid crystal (LC) is a substance which flows like a liquid but has some degree of ordering in the arrangement of its molecules. The LC doesn't have a positional order but has an orientational order, so it may flow like a liquid, but its molecules may be oriented in a crystal-like way. The peculiar characteristics of a LC is that it is anisotropic in nature; optical and other properties such as thermal and electrical conductivity vary with direction. The anisotropy of liquid crystals causes them to exhibit birefringence, i.e. when the light enters the crystal, it breaks up into two oppositely polarized rays which then travel at different velocities. The colorful patterns can be observed by placing the birefringent materials in between two crossed polarizers.

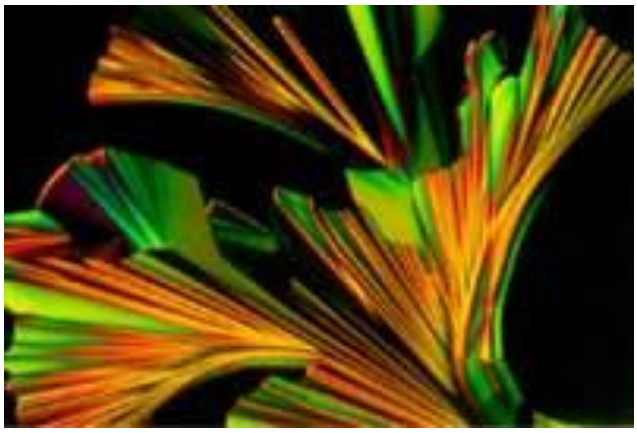

Figure 1.1 Colorful patterns in LCs

Since the extraordinary ray traverses a slightly longer path through the material and thus emerges later (and out-of-phase) than the ordinary ray, there exists an interference between these two rays which leads to the colorful patterns.

1.2 Nematic Phase of LCs

Among many phases of LCs, currently we are working on the Nematic phase. In a *nematic phase* (the term means "thread-like") the molecules are aligned in the same direction but are free to drift around randomly, very much as in an ordinary liquid. The alignment of the rod-like molecules can be controlled by the application of an external stimuli, such as optical, electrical, and mechanical.

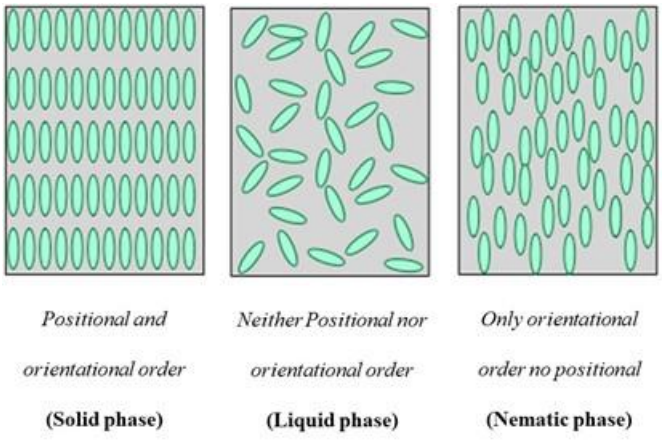

Figure 1.2 Molecular ordering in materials

Thermotropic nematic liquid crystals are subject to thermal expansion and possess a mesophase only within a certain temperature range. As the temperature rises, the average spacing between the aligned molecules increases, thus causing the e-ray to be increasingly retarded with respect to the o-ray, because of which the nematic phase changes into isotropic phase.

1.3 Topological Defects and Disclinations network

Topological defects are the positions where the molecular orientation cannot be defined but can control the alignment and dynamics of the LCs. The disclinations are topological singularities of molecular arrangement in liquid crystals, or simply defects in the orientation of a *director*; a common axis where all the molecules intend to orient.

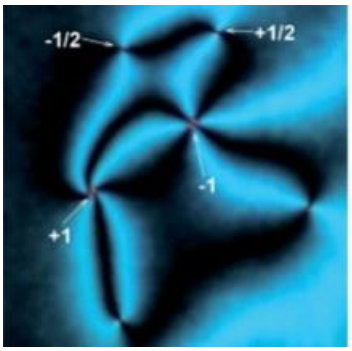

Figure 1.3 Defects and strengths in LCs[1]

Defects are local breakings of symmetry in an ordered medium. Disclinations break rotational symmetries and are the basic defects of media with continuous symmetries, like liquid crystals. The strength of a defect can be defined as the number of brushes divided by four (+ for clockwise rotation of brushes and – for counter-clockwise).

1.4 Motivations for the project

In 2010, Xiubo Zhao et al. explored the advances in studying peptide amphiphiles, focusing on the formation of different nanostructures and their applications in diverse fields. Many interesting features learned from peptide self-organisation and hierarchical templating will serve as useful guidance for functional materials design and nanobiotechnology. In 2011, Rajesh Chakrabarty et al. demonstrated the uses and applications of the self-assembled metallacycles and metallacages. Both 2D and 3D systems have been used in chemosensing and host-guest chemistry,

particularly interesting are use of 3D cages for the encapsulation of reactive species as described above. However, the most recent and arguably interesting applications have been in catalysis, use as microreactors and biological applications. In 2015, Wang. et al. found that the local nano-environments created by singular topological defects formed in LCs can be used to trigger and template cooperative processes involving the self-assembly of molecular amphiphiles. This finding expands the potential utility of defects for materials synthesis into the realm of molecules and nanoscopic molecular assemblies. In 2016, Y. Guo et al. designed a plasmonic photopatterning technique for aligning the molecular orientation in liquid crystals (LCs) in patterns with designer complexity. Using plasmonic metamasks in which target molecular directors are encoded, LC alignments of arbitrary planar patterns can be achieved in a repeatable and scalable fashion with unprecedentedly high spatial resolution and high throughput. In 2016, C. Peng et al. demonstrated an approach to control active matter through a patterned anisotropic environment. Self-propelled bacteria sense the imposed patterns of orientational order by adapting their spatial distribution, heading toward topological defects of positive charges and avoiding negative charges, and switching from bipolar locomotion in splayed and bent environments to unipolar locomotion in mixed splay-bend regions. In 2017, Hiroshi Yokoyama et al. has demonstrated the artificial creation of web of free-standing twist disclination lines in nematic LCs by engineering the patterned surface alignment so as to control the forces between disclination lines. The out-of-plane orientation of the director can be efficiently suppressed by using LCs with a negative dielectric anisotropy under a sufficiently intense electric field. In 2020, Harkai et al. demonstrated numerically and experimentally external electric field driven rewiring of a complex network of nematic line defects among competing configurations that are truly multi-stable, i.e., the new

configurations survive even when the field is switched off. They also illustrated the diversity of multi-stable and switchable configurations using an N×N array of charge ±1 defect for N = 4.

1.5 Objectives of the study

Here are few objectives that we will be seeking to follow:

Objective 1. Use complex photo-patterning technique to fabricate artificial defect lines.

Objective 2. Obtain biomolecular self-assembly by using nematic LC defect lines as templates.

Objective 3. Produce arbitrary and scalable geometry of biomolecular assembly.

Objective 4. Reconfigure the obtained biomolecular self-assembly into different geometry.

Chapter 2. Self-assembly of biomolecules triggered by the active nematic disclinations network.

2.1 Introductions

Molecular self-assembly describes spontaneous self-organization of building blocks from molecular level into complex and ordered superstructures [2-4]. Due to the recent development of biotechnology, genetic engineering and materials engineering, tremendous advances have been made to produce novel soft materials by using molecular building blocks such as peptides, fatty lipids, phospholipids and DNA [3,4]. Controlling the spontaneous molecular self-assembly into nanoscopic structures has been employed to realize a diverse range of functional nano-biomaterials for nanoscience, nanotechnology and nanomedicine [2-4]. Current methods are based on directed self-assembly involving self-association on multiple length scales[4,5] and employing external fields or chemical constraints to guide assembly route [3]. Using anisotropic fluid, such as liquid crystals (LCs), is a powerful alternative approach to generate a plethora of molecular self-assemblies which is not possible using conventional methods in isotropic solution. The nature of molecular interactions in LC is anisotropic and thus complexity of superstructures can be dramatically enriched [6]. Topological defects in LCs have shown promises to direct the self-assembly of colloids at the mesoscale in the cases such as directing particles to assemble clusters [7-13], mediating interactions of particles with flat [14], curved [15], and templated interfaces [16,17] and trapping at topological defects [18-22]. The possibility of using the nanoscopic environments created by defects in LCs to direct reversible assemblies of molecules was recently explored by Wang et al [23]. Topological defects in LCs show great potential as a versatile class of dynamic and reconfigurable templates for directing the molecular self-assembly in a predesigned manner.

In this work, we demonstrate that predesigning the nematic LC molecular orientation patterns by using the photo-patterning technique, different configurations, geometries and arbitrary shapes of linear defects-disclinations can be created. When amphiphiles are dispersed in the LC medium, self-assembly of molecules is triggered in the nanoscopic environments of disclination lines in a deterministically predesigned manner. Due to the sensitivity of LC to external stimuli, the created molecular assembly can be reconfigured by light and mechanical shear.

Nematic LC disclination lines are generated by assembling two substrates with different LC orientations. One substrate has topological orientation patterns made by photo-patterning [24,25], Fig. S1. The other substrate has uniform planar alignment fabricated by shining a linearly polarized light on the azo-dye coated substrate, see Methods. These two substrates are assembled with 20 μm glass spacers, Fig. 1b. We use amphiphiles labelled with dipyrrometheneboron difluoride (BODIPY), namely BODIPY-C5, mixed with nematic liquid crystal 5CB, Fig. 1a. The singly dispersed BODIPY-C5 can be imaged by using excitation light at 460-495nm and emission at 510-550nm, whereas the amphiphilic assembly signal can be detected from excitation at 510-550 nm and emission at 590- 630nm. This mixture is injected into the cell by capillary force at 45 ^{o}C which corresponds to the isotropic phase of 5CB. After the sample is cooled to room temperature, the disclination lines form.

2.2 Experimental Set-up and Procedure

2.2.1 Materials

5 CB is a common name for 4-Cyano-4'-pentylbiphenyl with the chemical formula $C_{18}H_{19}N$, which is a commonly used nematic liquid crystal. The liquid crystal 5CB undergoes a phase transition from a crystalline state to a nematic state at 24 °C and it goes from a nematic to an isotropic state at 35 °C. It has the density of 1.008 g/mL and molar mass of 249.357 g/mol. It appears cloudy white in nematic phase while colorless in isotropic phase.

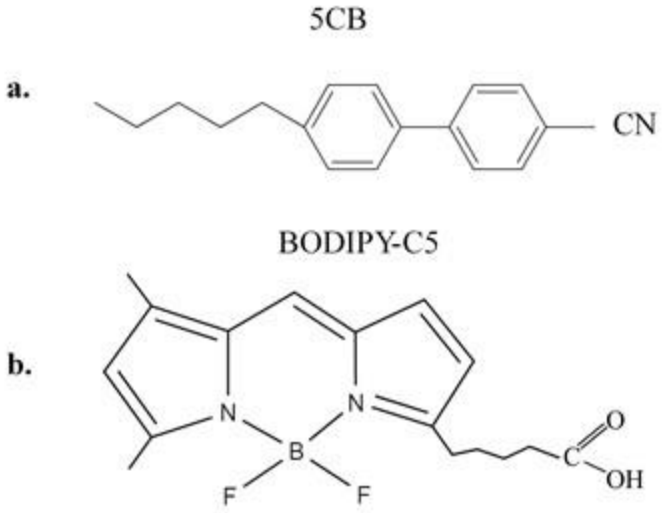

Figure 2.1 Chemical structure of materials used

Fluorescence labelled fatty acid 4,4-Difluoro-5,7-Dimethyl-4-Bora-3a,4a-Diaza-s-Indacene-3-Pentanoic Acid (BODIPY-C5), Fig. 1a, purchased from *Molecular Probes*. The singly dispersed BODIPY-C5 can be imaged by using excitation light at 460-495nm and emission at 510-550nm, whereas the amphiphilic assembly signal can be detected from excitation at 510-550 nm and emission at 590nm to 630nm. BODIPY-C5 is mixed with ethanol at 1 mg/mL. 3 μL of this solution is added to 125 μL of methanol. Then 125 μL of nematic liquid crystal 4′-pentyl-4-cyanobiphenyl (5CB), Fig. 1a, is added to the BODIPY-C5/methanol

solution. This mixture is sonicated for 30min and then dried in the vacuum oven at 60 ^{o}C overnight to remove the excess ethanol and methanol. Finally, a mixture of BODIPY-C5 in 5CB at 80 μM is obtained. Note that this concentration is above the critical assembly concentration (CAC) of 59 μM [23].

2.2.2 The Photo-patterning Set-up

The meta-mask is made of aluminum films of 150 nm thickness, perforated with rectangular nano-slits, each of a length 220 nm and width 100 nm. An unpolarized light beam passing through the slits of the photomask becomes linearly polarized; polarization of light is perpendicular to the long side of the slit. Since the orientation of slits is different from point to point in the mask, the light polarization also varies in space, as designed to achieve the desired director alignment. The pattern of polarized light transmitted through the photomask is projected onto the glass substrates coated with azo-dye using the projected system made of two microscope objectives (magnifications 5x and 50x), Fig. 2.2. The exposure time is 5 min. Afterwards, the polarization pattern is imprinted into the azo dye layer. The photoaligned liquid crystal shows the resulting director that is parallel to the local directions of the long axes of slits in the plasmonic photomask. The approach allows one to create any pattern of the director field with the typical scale of spatial gradients ranging from about 1 micrometer to hundreds of micrometers.

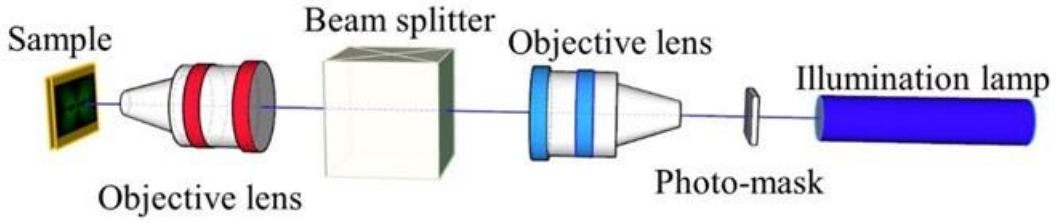

Figure 2.2 Schematic of patterned substrate preparation

2.2.3 Sample Preparation

a. Preparation of photopatterned substrates.

We followed the recently developed approach for surface photoalignment that is based on plasmonic photomasks used to irradiate the bounding plates with a light of controlled polarization pattern, described in details in Refs. [25,26]. The photosensitive material azo dye LIA-01 (from *DIC*) is mixed with N, N-Dimethylformamide (DMF) solvent at 0.2 wt% concentration. Glass substrates are washed according to the regular glass cleaning procedure. Glass substrates are washed in ultrasonic bath with detergent, then with isopropyl alcohol and dried in the oven at 80°C for 15 minutes. Subsequently the substrates are treated by oxygen plasma for about 5 minutes. The dye solution is spin coated on the glass substrates at 3000 rpm for 30s. The glass plates are then baked at 120^{o}C for 15 min. We used an X-Cite 120 metal halide lamp as a source of non-polarized light to illuminate the plasmonic meta-mask; the lamp output is the strongest in the spectral range between 350 nm and 450 nm.

b. Polymerization of RM257 monomer onto the pattern

A passivation layer with liquid crystalline polymer is used to preserve this pattern. Mesogenic reactive monomer RM257 is a polymerizable liquid crystal purchased from *Wilshire Technology INC*. RM257 and photo-initiator Irgacure 651 (from *Ciba*) are mixed with toluene at the concentration of 7 wt% and 0.3 wt%, respectively. This solution is spin-coated onto the photo-exposed azo-dye substrates at 3000 rpm for 30 s.

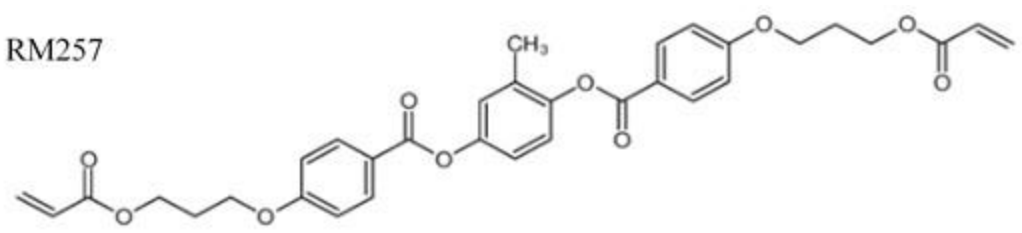

Figure 2.3 Chemical structure of RM257

The monomer is photopolymerized y an unpolarized UV light (UVL-26 Handheld UV lamp, *Analytikjena LLC*) with the intensity 1.4 mW/cm^2, wavelength 365 nm, for 30 min. The polymer pattern replicates the alignment pattern of azodye beneath it and a birefringent pattern will be shown due to the director field. Upon coating on the photo-patterned substrate, the polymerizable material RM257 is aligned through the interaction of RM257 molecules with the orientationally ordered chemical groups on the azo-dye layer. After UV polymerization of RM257, the microscale alignment patterns are well manifested in the RM257 polymer film.

c. Preparation of uniformly aligned substrate

Another substrate with uniform planar alignment is fabricated by shining a nonpolarized light on the azo-dye coated substrate through a linear polarizer. The planar alignment is perpendicular to the linear polarization. This planar substrate is assembled with the photo-patterned substrate and the gap is set by 20 μm glass spacers, Fig. 1b. The mixture of BODIPY-C5 in 5CB is injected into the cell by capillary force at 45 ^{o}C which corresponds to the isotropic phase of 5CB. After the sample is cooled to room temperature, the disclination lines form and the sample will be imaged by polarizing optical microscope and fluorescence optical microscope.

2.2.4 Descriptions of Microscopes Used

a. Polarizing optical microscopy

We used 50X-1000X Advanced Upright Polarizing Optical Microscope form *Amscope* with both 10x Plan, N.A.= 0.25 objective and 20x Plan, N.A.= 0.40 objective. Optical microscopic images are captured by 20MP USB3.0 BSI C-mount Microscope Camera from *Amscope.* (resolution 5440×3648 pixels).

b. Fluorescence optical microscopy

40X-1000X Upright Fluorescence Microscope with Rotating Multi-filter Turret form *Amscope* with both 10x Plan, N.A.= 0.25 objective and 20x Plan, N.A.= 0.40 objective. Filter cube used excitation and emission filters that transmitted light with wavelengths of 510nm to 550nm (ex: 510-550 nm) and 590nm to 630nm (em: 590-630 nm), respectively. The fluorescence illumination lamp used is X-Cite 120 from *Excelitas Technologies*.

2.3 Experimental Results

2.3.1 Creation of disclination lines

The director fields $\hat{\mathbf{n}}$ with topological defects are designed using a general formula $\hat{\mathbf{n}} = \left(n_x, n_y, n_z\right) = \left(\cos\theta, \sin\theta, 0\right)$, where $\theta\left(x, y\right) = m\tan^{-1}\dfrac{y}{x} + \theta_0$, where m is the integer or semi-integer topological charge, the phase θ_0 sets the type of distortions, either pure bend $\theta_0 = \pi/2$, or pure splay, $\theta_0 = 0$. For the circular +1 defect with pure bend, Fig. 2.4a, the birefringent pattern after coated with liquid crystalline polymer RM257 is shown in Fig. 2.4b. After this substrate is assebmled with another substrate with uniform planar alignment in x direction, Fig. 2.4c, polarizing microscope image of the formed disclination lines is shown in Fig. 2.4d.

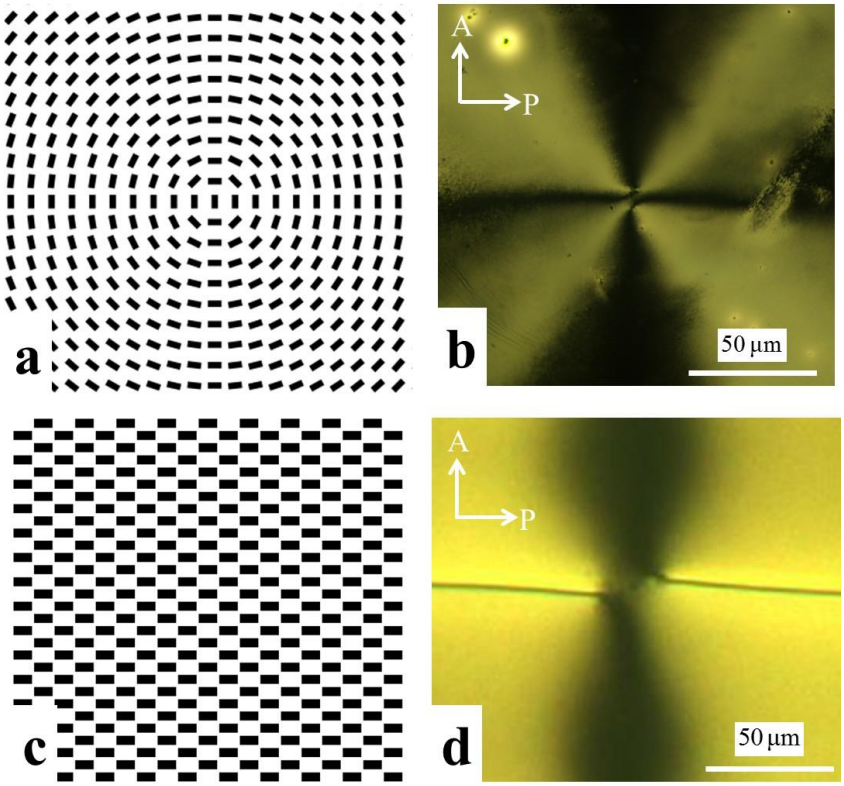

Figure 2.4 Polarizing microscopic images of disclination line from circular +1 defect

(**a**) Director field of this circular +1 director pattern with pure bend deformation; (**b**) Polarizing microscopic image of the pattern; (**c**) Uniform alignment along x-axis; (**d**) Polarizing microscopic image of the disclination lines formed in the assembled sample with patterned and uniform alignment substrates; P and A represent the directions of polarizer and analyzer.

A topological defect pair (+1/2, -1/2) is created by $\theta(x,y) = m_1 \tan^{-1}\frac{y}{x} + m_2 \tan^{-1}\frac{y}{x-l}$,

where $m_1 = 1/2$, $m_2 = -1/2$ and $l = 50\mu\text{m}$ is the distance between the defect cores, Fig. 2.5a. The polarizing micrograph of this pattern is shown in Fig. 2.5b. After assembling this patterned substrate with the uniform aligned substrate, the disclination lines are created, Fig. 2.5c-d.

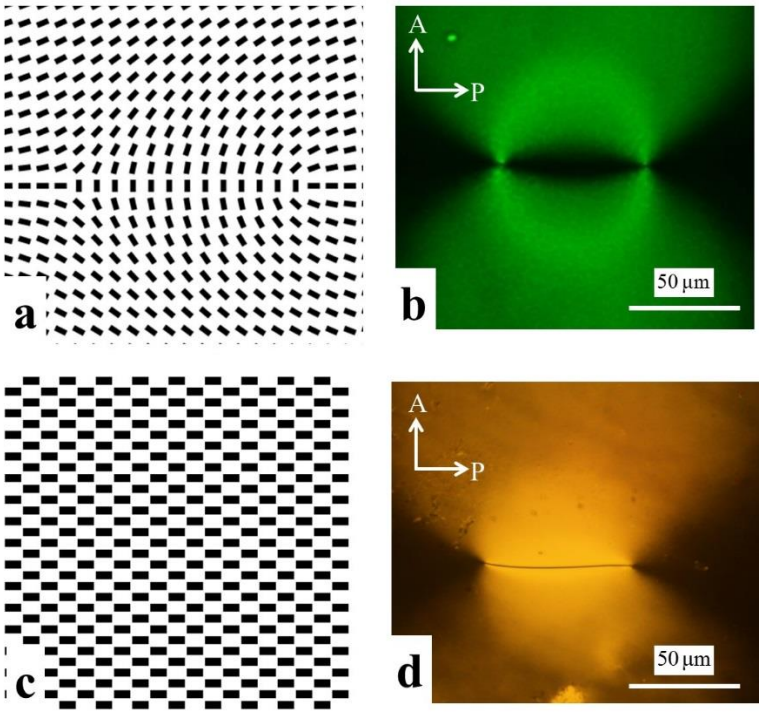

Figure 2.5 Polarizing microscopic images of disclination lines from defect pair (+1/2, -1/2)

(**a**) Director field of pattern with defect pair (+1/2, -1/2); (**b**) Polarizing microscopic image of the pattern; (**c**) Uniform alignment along x-axis; (**d**) Polarizing microscopic image of the disclination lines formed in the assembled sample with patterned and uniform alignment substrates; P and A represent the directions of polarizer and analyzer.

A more complex topological defect with strength of +3/2 is designed by $\theta(x,y) = m\tan^{-1}\frac{y}{x} + \theta_0$, where $m = 3/2$ and $\theta_0 = 0$, Fig. 2.6a. The polarizing micrograph of this pattern is shown in Fig. 2.6b. After assembling this patterned substrate with the uniform aligned substrate, the disclination lines are created, Fig. 2.6c-d.

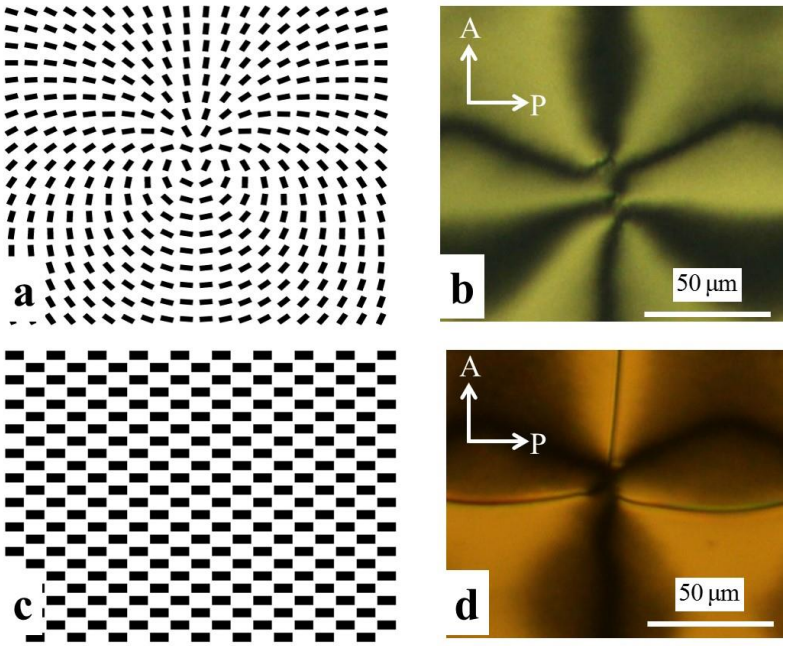

Figure 2.6 Polarizing microscopic images of disclination lines from defect charge of 3/2

(**a**) Director field of this pattern with defect charge of 3/2; (**b**) Polarizing microscopic image of this pattern; (**c**) Uniform alignment along x-axis; (**d**) Polarizing microscopic image of the disclination lines formed in the assembled sample with patterned and uniform alignment substrates; P and A represent the directions of polarizer and analyzer.

By using photopatterning technique, disclination line network is also created. A 2D lattice of alternating +1/2 and -1/2 topological defects are designed with $\theta(x,y)=\sum_i m_i \tan^{-1}\frac{y-y_{i0}}{x-x_{i0}}+\theta_0$, where $m_i=1/2$, $m_{i+1}=-1/2$, $\theta_0=0$ and $x_{i0}=y_{i0}=50\mu m$ is the distance between the defects, Fig. 2.7a. The polarizing micrograph of this pattern is shown in Fig. 2.7b. After assembling this patterned substrate with the uniform aligned substrate, the disclination lines are created, Fig. 2.7c-d.

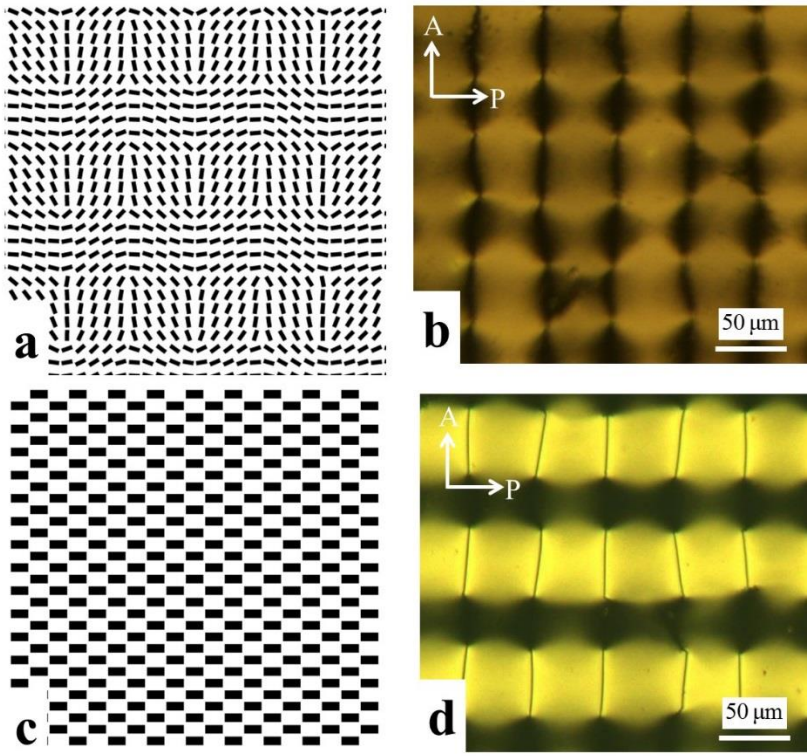

Figure 2.7 POM images of a 2D disclination line network from defect array of (+1/2, -1/2)

(**a**) Director field of the 2D lattice of alternating +1/2 and -1/2 topological defects; (**b**) Polarizing microscopic image of this pattern; (**c**) Uniform alignment along x-axis; (**d**) Polarizing microscopic image of the disclination lines formed in the assembled sample with patterned and uniform alignment substrates; P and A represent the directions of polarizer and analyzer.

Different configurations of disclination line network are also created. A 2D lattice of alternating +1 and -1 topological defects are designed with $\theta(x,y)=\sum_i m_i \tan^{-1}\frac{y-y_{i0}}{x-x_{i0}}+\theta_0$, where $m_i=1$, $m_{i+1}=-1$, $\theta_0=\pi/2$ and $x_{i0}=y_{i0}=100\mu m$ is the distance between the defects, Fig. 2.8a. The polarizing micrograph of this pattern is shown in Fig. 2.8b. After assembling this patterned substrate with the uniform aligned substrate, the disclination lines are created, Fig. 2.8c-d.

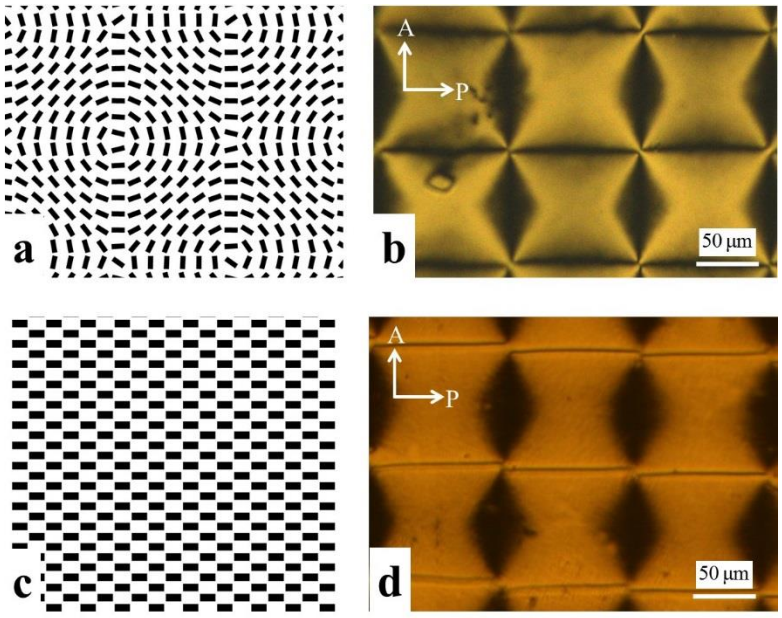

Figure 2.8 POM images of a 2D disclination line network from defect array of (+1, -1)

(**a**) Director field of the 2D lattice of alternating +1 and -1 topological defects; (**b**) Polarizing microscopic image of this pattern; (**c**) Uniform alignment along x-axis; (**d**) Polarizing microscopic image of the disclination lines formed in the assembled sample with patterned and uniform alignment substrates; P and A represent the directions of polarizer and analyzer.

Surface patterning offers a broad freedom in the design of disclination line network with different geometry. For example, a two-dimensional array of topological defects is designed in the form

$$\theta(x,y)=\sum_{m,n}\left[\tan^{-1}\frac{y+d_m}{x+d_n}-\frac{1}{2}\left(\tan^{-1}\frac{y+d_m}{x+d_n+d}+\tan^{-1}\frac{y+d_m}{x+d_n-d}\right)\right]+$$
$$\sum_{p,q}\left[\tan^{-1}\frac{y+d_p}{x+d_q}-\frac{1}{2}\left(\tan^{-1}\frac{y+d_p}{x+d_q+d}+\tan^{-1}\frac{y+d_p}{x+d_q-d}\right)\right] \quad ,$$

$$d_m=\sqrt{3}md\,, \qquad m=0,\pm1,\pm2\ldots, \qquad d_n=3nd\,, n=0,\pm1,\pm2\ldots, d_p=\frac{\sqrt{3}}{2}(2p+1)d\,,$$

$p=0,\pm1,\pm2\ldots, d_q=\frac{3}{2}(2q+1)d\,, q=0,\pm1,\pm2\ldots,$ and d is the distance between the defects of strength 1 and -½. Typical values of *m*, *n*, *p*, and *q* in the photomasks were 4-5., Fig. 2.9a. The polarizing micrograph of this pattern is shown in Fig. 2.9b. After assembling this patterned

substrate with the uniform aligned substrate, the disclination lines are created, Fig. 2.9c-d. The dispersed amphiphile molecules will self-assembly in these predesigned disclination line network.

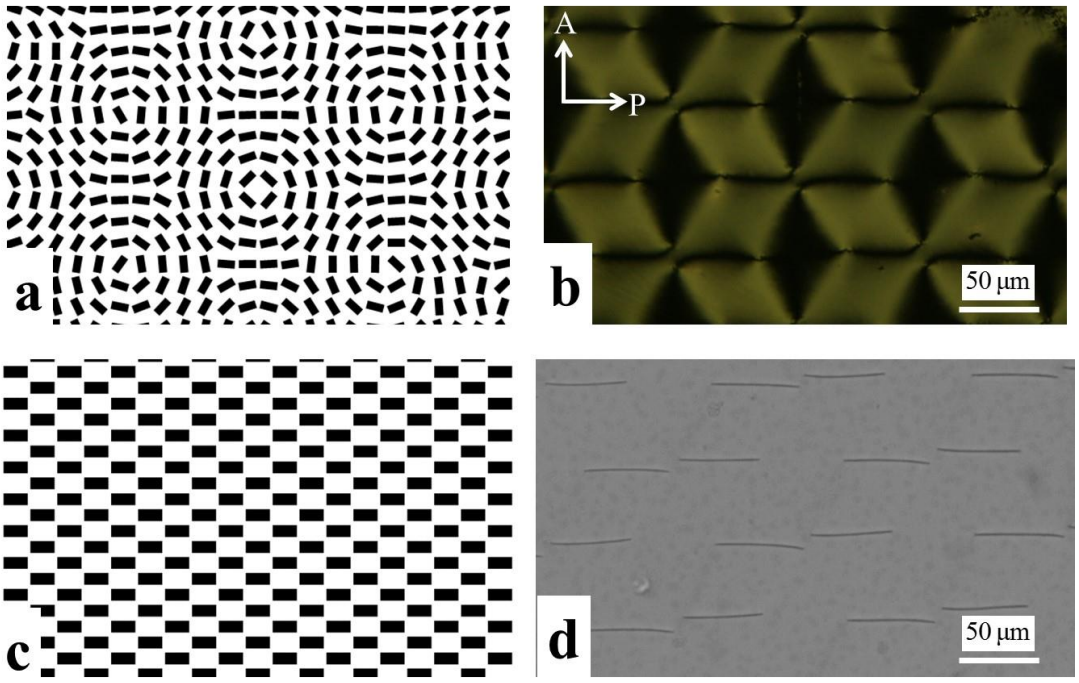

Figure 2.9 Micrographs of a hexagonal arrangement of disclination lines

(**a**) Director field of this hexagonal pattern; (**b**) Polarizing microscopic image of this pattern; (**c**) Uniform alignment along x-axis; (**d**) Bright-field microscopic image of the hexagonal arrangement of disclination line network formed in the assembled sample with patterned and uniform alignment substrates; P and A represent polarizer and analyzer.

Disclination line networks can also be created without topological defects. A 2D director field with periodic splay and bend deformations is designed in the form with $\theta(y) = \pi y / l$, where $l = 80\ \mu\text{m}$ is the period, Fig. 2.10a. The polarizing micrograph of this pattern is shown in Fig. 2.10b. After assembling this patterned substrate with the uniform aligned substrate, continuous straight disclination lines are created, Fig. 2.10c-d. Amphiphilic assembly with periodicity of $80\ \mu\text{m}$ are generated following the straight disclination lines, Fig. 2.10e.

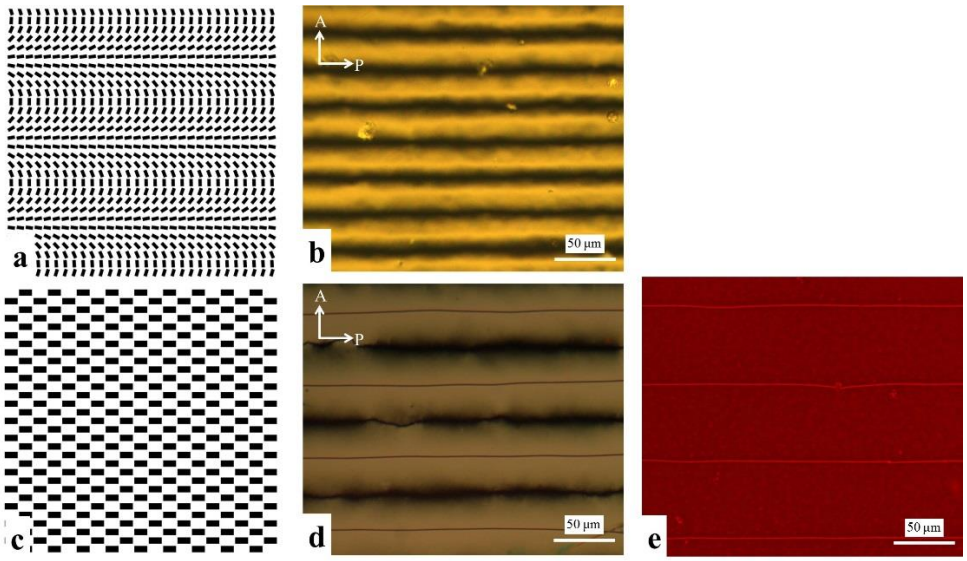

Figure 2.10 Micrographs of straight disclination lines by a pattern with periodic splay and bend deformations

(**a**) Director field of the periodic pattern; (**b**) Polarizing microscopic image of this pattern; (**c**) Uniform alignment along x-axis; (**d**) Polarizing microscopic image of the straight disclination lines formed in the assembled sample with patterned and uniform alignment substrates; (**e**) Fluorescence micrograph of formed amphiphilic assemblies on the disclination lines; P and A represent the directions of polarizer and analyzer.

2.3.2 Self-assembly of biomolecules

Photoalignment azo-dye layer with director fields $\hat{\mathbf{n}}$ is designed using a general formula $\hat{\mathbf{n}} = \left(n_x, n_y, n_z\right) = \left(\cos\theta, \sin\theta, 0\right)$, where $\theta\left(x, y\right) = m_1 \tan^{-1}\dfrac{y}{x-d} + m_2 \tan^{-1}\dfrac{y}{x} + \theta_0$, where m_1 and m_2 set the charge of topological defects, the phase θ_0 sets the type of distortions, d is the distance between the defects. Fig. 2.11c shows that the pattern substrate has circular +1 defect structure with $m_1 = 0$, $m_2 = +1$ and $\theta_0 = \pi/2$. When assembled with uniform substrate along x-axis, LC director is forced to twist in opposite sense in the plane from the center of pattern to the edge [27]. In order to resolve this structural incompatibility in LC, singular disclination lines of strength 1/2 in x direction is formed and extended to the boundary of the pattern, Fig. 2.11d. When BODIPY-

C5 is mixed with LC and imaged by light at 510-550 nm, stronger signal at 590- 630nm is emitted from the disclinations, indicating that self-assembly of amphiphiles is triggered, Fig. 2.11e. Note that the concentration of BODIPY-C5 is above the critical assembly concentration (CAC) to ensure the self-assembly of molecules [23]. Different configurations of molecular assembly can also be designed. Fig. 2.11f shows a pattern with LC director field of (+1/2, -1/2) defect pair. Disclination lines connecting the defect pair are created, Fig. 2.11g, and the amphiphilic assemblies form in the predesigned lines, Fig. 2.11h. A more complex defect with topological charge of +3/2 is designed, Fig. 2.11i, and the amphiphilic assemblies follow the disclination line configurations, Fig. 2.11j-k. The fact that disclination lines connect 1/2 defects emphasizes the topological feature of the disclinations that are characterized by a strength of 1/2 in a nematic LC [28].

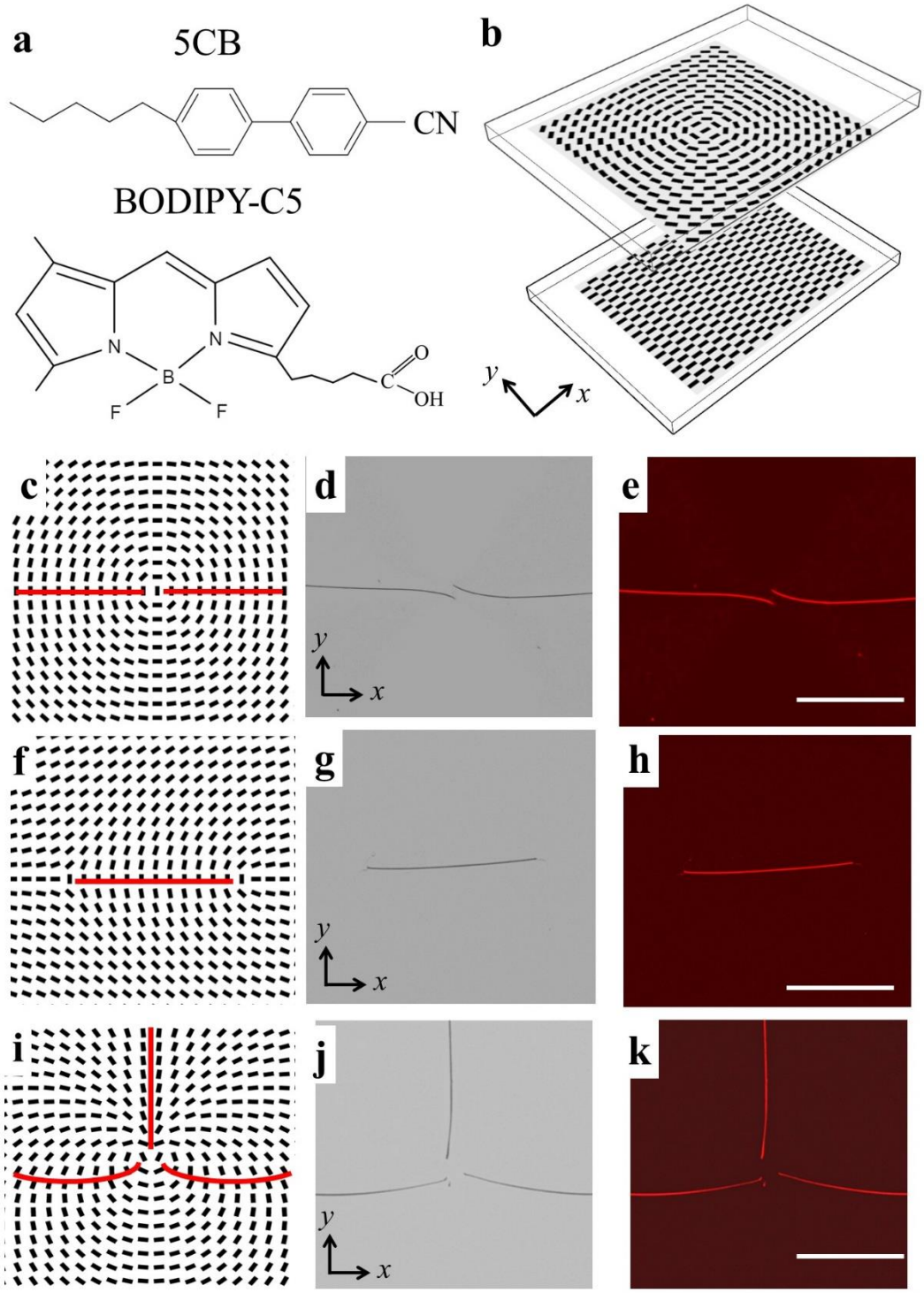

Figure 2.11 Templated molecular self-assembly by LC defect lines

(**a**) Molecular structure of nematic liquid crystal 5CB and amphiphile comprised of fatty acid C5 conjugated to BODIPY (BODIPY-C5); (**b**) Schematic of assembling two substrates; One with topological orientation pattern and the other with uniform orientation along x-axis; **(c)** Director field of the patterned substrate with circular +1 defect at the center; The red lines indicate the position of disclination lines; **(d)** Optical microscope image of formed disclinations lines; **(e)** Fluorescent microscope image of obtained BODIPY-labelled amphiphile assemblies; (**f**)-(**h**) Director field of (+1/2, -1/2) defect pair **(f)**, formed disclination lines (**g**) and fluorescence micrograph of amphiphile assemblies (**h**); (**i**)-(**k**) Director field of +3/2 defect **(i)**, formed disclination lines (**j**) and fluorescence micrograph of molecular assemblies **(k)** ; Scale bar $50\,\mu m$.

As a proof-of-capability of pre-designing different configurations of amphiphilic assemblies, more complex director fields are generated. A two dimensional (2D) lattice of alternating +1/2 and -1/2 topological defects are designed with $\theta(x,y)=\sum_i m_i \tan^{-1}\frac{y-y_{i0}}{x-x_{i0}}+\theta_0$, where $m_i=1/2$, $m_{i+1}=-1/2$, $\theta_0=0$ and $x_{i0}=y_{i0}=50\mu m$ is the distance between the defects, Fig. 2.12a. The amphiphile assemblies are templated into a 2D hierarchical structures following the formed disclination line array, Fig. 2.12b. The quantification of the fluorescence intensity in Fig. 2.12c reveals that the amphiphiles are precisely positioned in the local environment of defect line array. Note that the non-zero fluorescent intensity in the bulk LC is a background signal from the singly dispersed amphiphilic molecules [23]. A lattice of alternating +1 and -1 defects is also patterned, Fig. 2.12d. After assembled with a uniform substrate along x-axis, disclination lines and amphiphilic assemblies form, Fig. 2.12e. Note that the amphiphiles assemblies in Fig. 2.12a-c and Fig. 2.12d-f have different configurations due to the design of the 2D defect lattice. Fig 2.12a-c form 2D molecular assemblies with equal distance in both x and y directions, however, assemblies in Fig. 2.12d-f have equal distance along y-axis but connected in x direction. Different geometry of amphiphile assemblies can also be produced. A hexagonal arrangement of 2D lattice of defect triplet (-1/2, +1, -1/2) is designed, Fig. 2.12g. The disclination lines and the amphiphilic assemblies are formed following this hexagonal geometry, Fig. 2.12h-i.

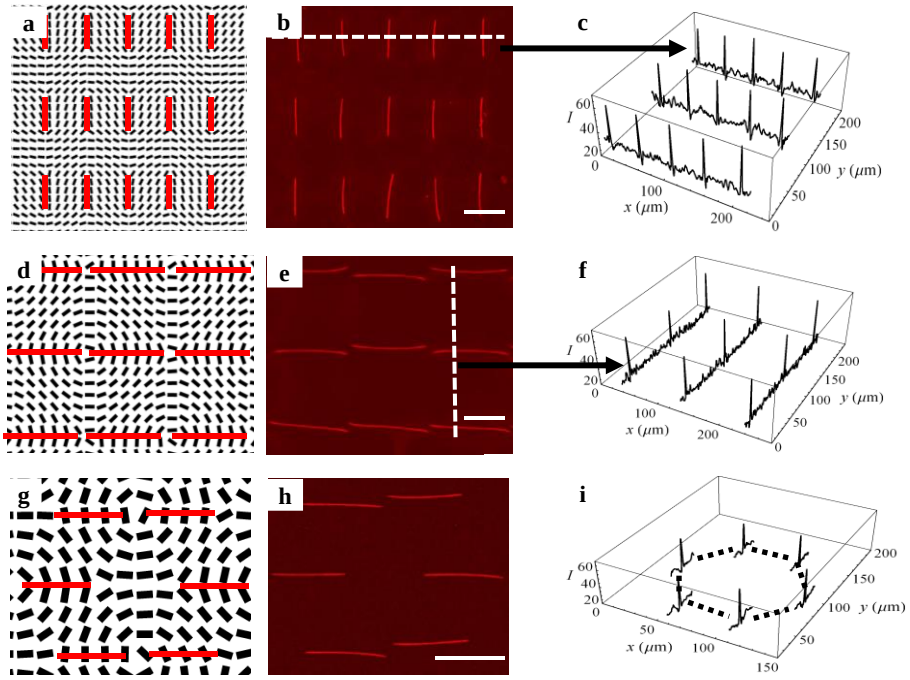

Figure 2.12 Predesigned self-assembly of amphiphiles in LC defect line array

Note that the substrate with uniform alignment along x-axis; **(a)** Director field of (+1/2, -1/2) defect array; The red lines indicate the position of disclination line array; **(b)** Fluorescent microscope image of BODIPY-labelled amphiphile assemblies in the disclination line array; **(c)** Measured fluorescence intensity (represented by I) across the line indicted in part (**b**); **(d)-(f)** Director field of (+1, -1) defect array (**d**), fluorescence micrograph of amphiphilic assemblies in the defect line array(**e**) and measured fluorescence intensity across the lines (**f**); **(g)-(i)** Director field of hexagonal geometry of defect array (**g**), formed disclination line array (**h**), fluorescence micrograph of molecular assemblies (**i**) and hexagonal geometry of measured fluorescence intensity across the lines (**h**); Scale bar is $50\,\mu m$.

Arbitrary shapes of amphiphilic assemblies can be created by programming the patterns. For example, when the director field is designed as $\theta(x,y)=\sqrt{x^2+y^2}$, Fig. 3b, and assembled with a uniform substrate along y-axis, amphiphilic assemblies with the shape of letter "O" is formed, Fig. 2.13e. Amphiphilic assemblies with shape of letter "U" and "M" are created respectively by taking the topological pattern $\theta(x,y)=m_1\tan^{-1}\frac{y}{x-d}+m_2\tan^{-1}\frac{y}{x}+m_3\tan^{-1}\frac{y}{x+d}$ with $m_1=+1.5$, $m_2=-1.5$, $m_3=0$ and $d=100\,\mu\text{m}$ for letter "U", Fig. 3a and d, and $m_1=-1.5$, $m_2=+1.5$ and $m_3=-1.5$ for letter "M", Fig. 3c and f. 3D mapping of the fluorescence intensity of amphiphilic assemblies show that molecules only self-assemble in the disclinations in the form of letters "*UOM*".

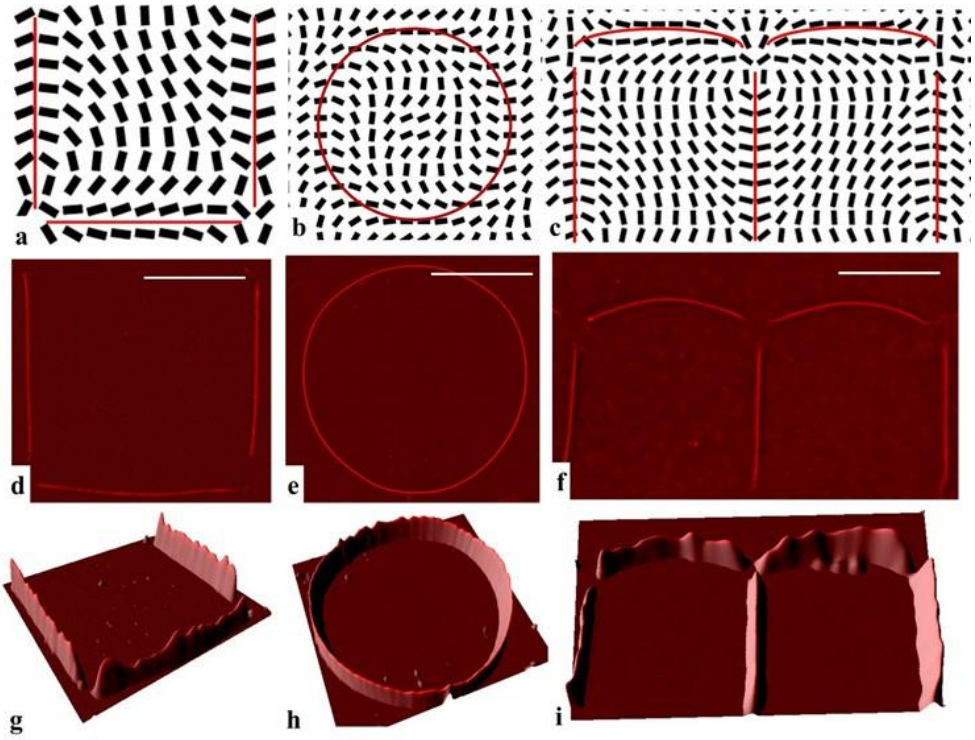

Figure 2.13 Arbitrary shapes of self-assembly of amphiphiles in LC defect lines

Note that the substrate with uniform alignment along y-axis; (**a**)-(**c**) Director field of the patterned substarte to make letters "U" "O" "M" disclination lines respectively; (**d**)-(**f**) Fluorescence micrograph of amphiphilic assemblies in the form of letters "UOM"; (**g**)-(**i**) 3D fluorescence intensity mapping of letters "UOM". Scale bar is $50\ \mu m$.

Not only we can create the arbitrary shapes of disclination lines, but also obtain different geometries, such as changing the dimensions or lengths of the lines. By the same photo-patterning technique, we can obtain the defect lines twice as large as usual one, Fig. 2.14. For this, we just need to remove the objective lens from our set-up in order to imprint larger photopatterned image on the azodye substrate. Here, we have used two patterns, 1 array and (+1/2, -1/2) defect pair, to demonstrate the idea of creating scalable defect lines. Fig. 2.14a, b clearly shows the change in length of the defect lines at least twice in the (+1/2, -1/2) defect pair, and Fig. 2.14c, d confirms that the lines are scalable in the pattern of strength 1 array as well.

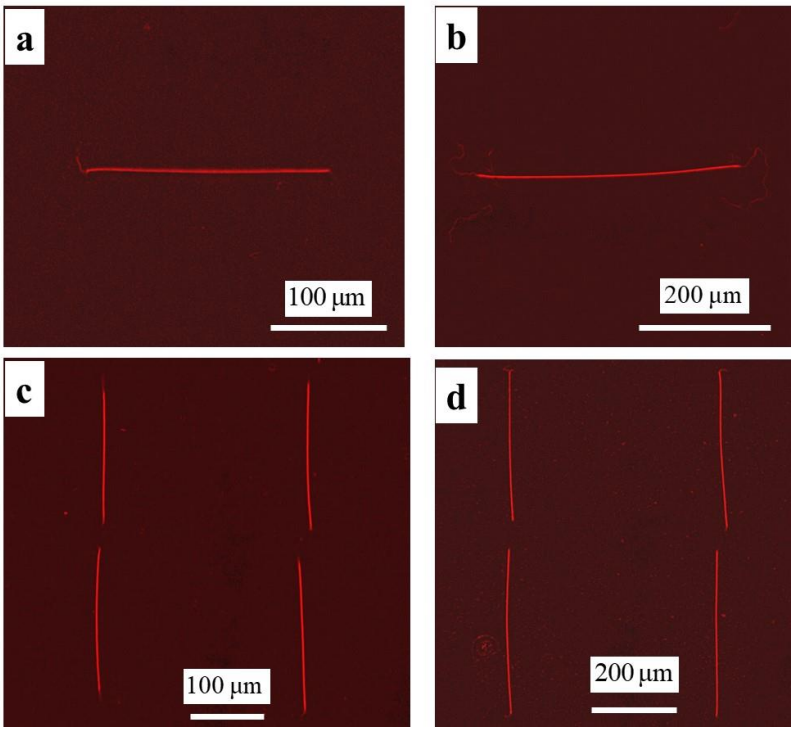

Figure 2.14 Extending the molecular self-assembly into different length scales

(a), (b) Fluorescence micrographs of self assembly of lipids in the pattern of strength (+1/2, -1/2) defect pair with scalebars 100 μm and 200 μm respectively. (c), (d) Self-assembly of the biomolecules in the pattern of strength 1 array with scalebars 100 μm and 200 μm respectively.

Since one substrate of the sample is aligned uniformly with azodye photoalignment layer, it expands the capability to reconfigure the molecular assembly by using light illumination, Fig 2.15. Fig. 2.15a shows that initial configuration of amphiphiles along x-axis with the uniform substrate aligned in x direction. When a linearly polarized light along x-axis is shone through the uniform azo-dye substrate, the azo-dye layer will be realigned perpendicularly to the linear polarization, i.e. y-axis, so that the defect line array would change the configuration from x-axis to y-axis and amphiphilic assemblies in the defect lines follow this reconfiguration, Fig. 2.15b-c. Note that the other patterned substrate is coated with a passivation layer of liquid crystalline polymer so it is not changed by the light illumination, See Methods. Similar effects can also be realized by applying external stimuli such as mechanical shear. Fig. 2.15d-I show the dynamic change of amphiphilic assemblies by mechanical rotating the uniform aligned substrate from x-axis to y-axis. The initial state is along x-axis, Fig. 2.15d. Due to the reconfiguration of the disclination line network, the amphiphilic assemblies are transported following this dynamic motion, Fig. 2.15e-h, and the final amphiphilic assemblies are along y-axis, Fig. 2.15i. By simply using a linearly polarized light and mechanical shear, the reconfigurations of the molecular assemblies are easily induced by programming the defect lines template.

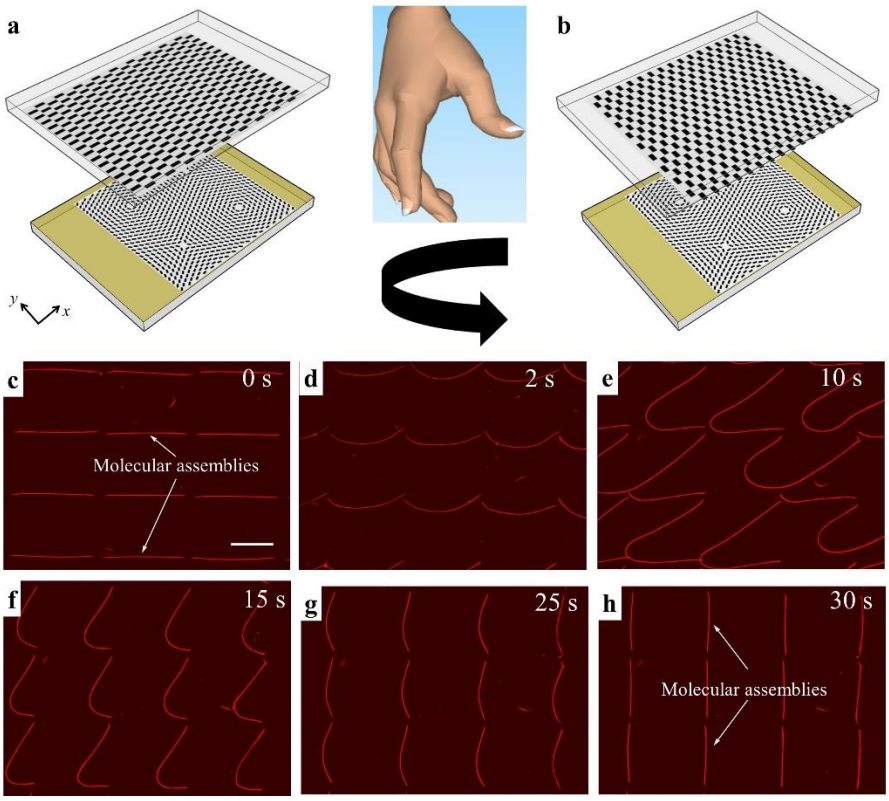

Figure 2.15 Reconfiguration of amphiphilic assemblies by light and mechanical shear

(**a**) Initial configuration of amphiphiles along x-axis due to the uniform substrate is aligned in x direction; (**b**)-(**c**) Amphiphilic configuration is changed to along y-axis by using mechanical force; (**d**)-(**i**) Time lapse of reconfiguration of the amphiphilic assemblies by mechanically rotating the top uniform substrate from x-axis to y-axis.

Chapter 3. Reconfiguration of the self-assembly of the amphiphiles by using Light.

3.1 Introductions

We have already demonstrated that by photopatterning nematic liquid crystal (LC), predesigned artificial defect line network is created, triggering molecular self-assembly in those nanoscopic environments. Now, it's time to show that the programmable molecular assembly structures can also be reconfigured by using external stimuli such as electric field, and light illumination. Previous work has been focused on creating artificial web of disclination lines in nematic liquid crystals [29] and electric field driven reconfigurable multistable topological defect patterns [30]. Along with the reconfiguration of the lines in different geometry, the nucleation and annihilation of the disclination loops has also been studied [31]. So, we try to demonstrate that the amphiphiles also follow the dynamics of the disclination loops using different technique. The technique to control and program and re-configurate the molecular self-assembly in predesigned locations and superstructures can be of importance for the development of dynamic functional nano-biomaterials, soft active materials, microfluidic, and sensing devices.

In this work, we demonstrate that predesigning the nematic LC molecular orientation patterns by using the patterning technique, different configurations, geometries and arbitrary shapes of linear defects-disclinations can be created. When amphiphiles are dispersed in the LC medium, self-assembly of molecules is triggered in the nanoscopic environments of disclination lines in a deterministically predesigned manner. Due to the sensitivity of LC to external stimuli, the created molecular assembly can be reconfigured by light.

3.2 The patterning set-up

For this project, we used a different patterning setup for photopatterning the director fields in the sample. The patterning set up consists of the projector, two spherical lenses, a linear polarizer, an objective lens, and a sample holder, Fig. 3.1. The unpolarized light is rendered from the projector through two spherical lenses which converge the rays of light into a beam. The shape of the projection of the light can be controlled by a computer by using the ppt slides. The beam of a light is then passed through a polarizer which linearly polarizes the light, which eventually strikes the sample after passing through the objective lens. Here, the objective lens is used to focus the beam of light into the sample. We can rotate the polarizer and the projection of the light depending upon the strength of the pattern we desire. We can produce several patterns with different strengths simply by operating the mathematical formula, $M=R_1/R_2$, where M is the strength of the pattern, R_1 and R_2 are the rates of speed of rotation of the polarizer and the projection of light, respectively. As the pattern of polarized light transmitted through the polarizer is projected onto the glass substrates coated with azodye using a microscope objective (magnifications 5x), the polarization pattern is imprinted into the azo dye layer in around 3 min.

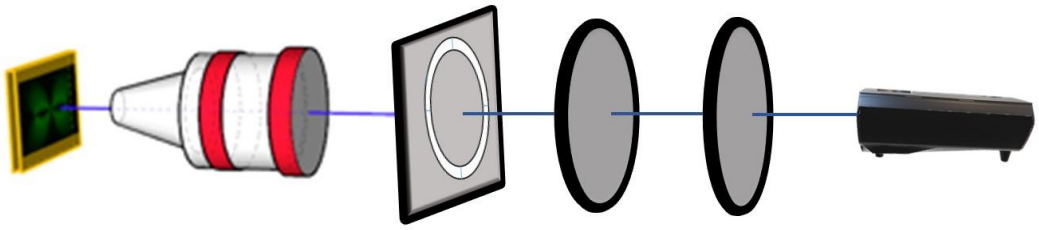

Figure 3.1 Schematic of patterned substrate preparation

3.3 Creating different patterns and the defect lines

The simple circular pattern with strength +1 is created by operating the formula $M=R_1/R_2$, using $R_1=1$ and $R_2 = 1$ we get M=1, which means the polarizer and the projection of light is rotated

through same angle in the same direction. In particular, a small segment of light in triangular shape of core angle 10 degree is projected into the sample and the sample was illuminated for around 5 sec. After every 5 sec, both the polarizer and the segment of the projected light is rotated by another 10 degree. In this manner, a whole circular pattern gets imprinted onto the azodye coated substrate after completing 360degree rotation. The birefringent pattern with red plate inserted after coated with liquid crystalline polymer RM257 is shown in Fig. 3.2b. After this substrate is assebmled with another substrate with uniform planar alignment in x direction, Fig. 3.2c, polarizing microscope image of the formed disclination lines is shown in Fig. 3.2d.

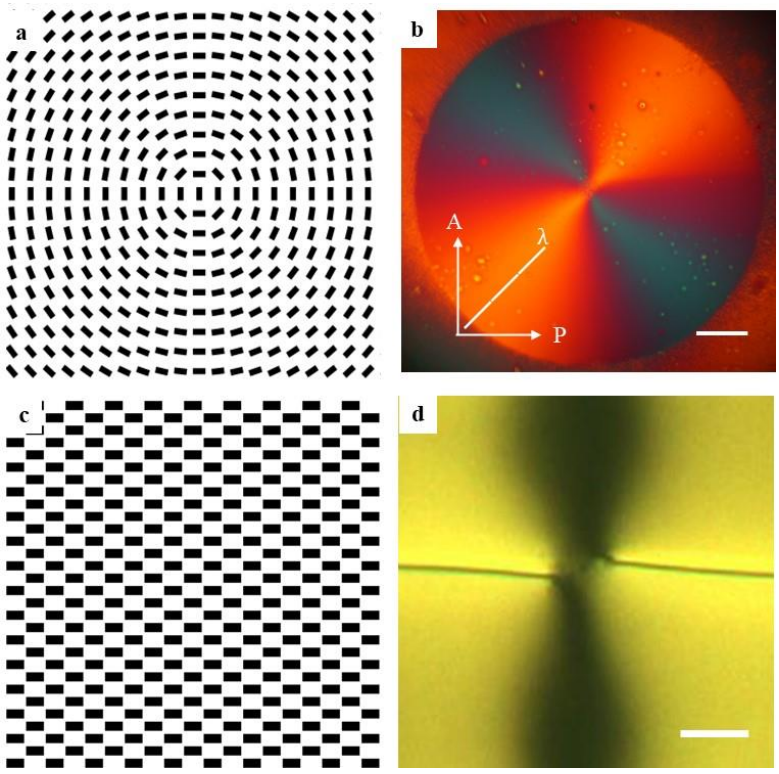

Figure 3.2 Polarizing microscopic images of disclination line from circular +1 defect

(**a**) Director field of this circular +1 director pattern with pure bend deformation; (**b**) Polarizing microscopic image of the pattern with the red plate inserted; (**c**) Uniform alignment along x-axis; (**d**) Polarizing microscopic image of the disclination lines formed in the assembled sample with patterned and uniform alignment substrates; P and A represent the directions of polarizer and analyzer. Scale bar is 200 μm.

In the similar way, we can produce an array of defects with strengths +1 and -1. In order to produce a defect with -1 strength, we need to rotate the polarizer and the projection of the light in the same amount in reverse direction. That means, if we rotate the polarizer in clockwise direction then the projection of the light should be rotated in the anti-clockwise direction. Here, in the Fig. 3.3a-b, we are showing a pattern consisting four defects with alternating +1 and -1 strength in an array. After assembling this patterned substrate with the uniform aligned substrate, the disclination lines are created, Fig. 3.3c. The 3D fluorescence intensity graph of the self-assembly of the molecules along the lines is plotted and shown in Fig 3.3d-f. The intensity peaks in the graphs also depicts how the lines change with the applied optical field and thus the self-assembly of molecules as well.

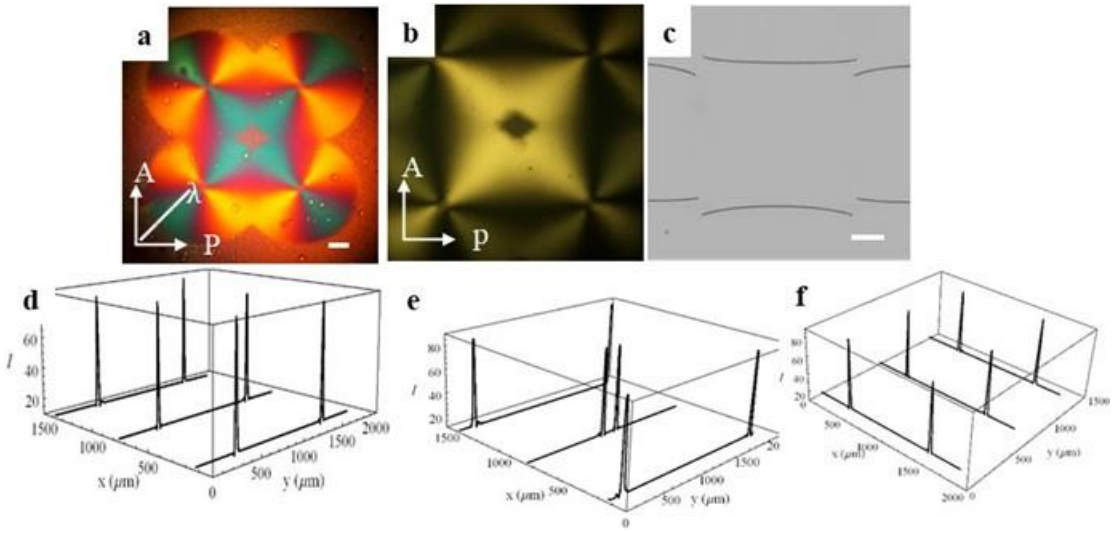

Figure 3.3 POM images of disclination lines from a pattern of Strength 1 array

(**a**), (**b**) Polarizing microscopic image of the pattern with red plate and without red plate, respectively; (**c**) Polarizing microscopic image of the disclination lines formed in the assembled sample with patterned and uniform alignment substrates; (**d**)-(**f**) Fluorescence intensity graphs of the self-assembly of the molecules along the lines of interest; P and A represent the directions of polarizer and analyzer.

A more complex pattern with defect strength +1/2 and -1/2 is created by using R_1=1 and R_2=2 in the abovementioned formula. That means, the projection of light is rotated with twice the speed of the rotation of the polarizer. In particular, the polarizer is rotated in every 10 sec while the projection of the light is rotated in every 5 sec to obtain the ratio of rotation speeds 1/2. The polarizing micrograph of the single +1/2 defect is shown in Fig. 3.4b-c, and the pattern of the alternating +1/2 and -1/2 defect strength is shown in Fig. 3.4f-g. After assembling this patterned substrate with the uniform aligned substrate, the disclination lines are created, Fig. 3.4d and 3.4h.

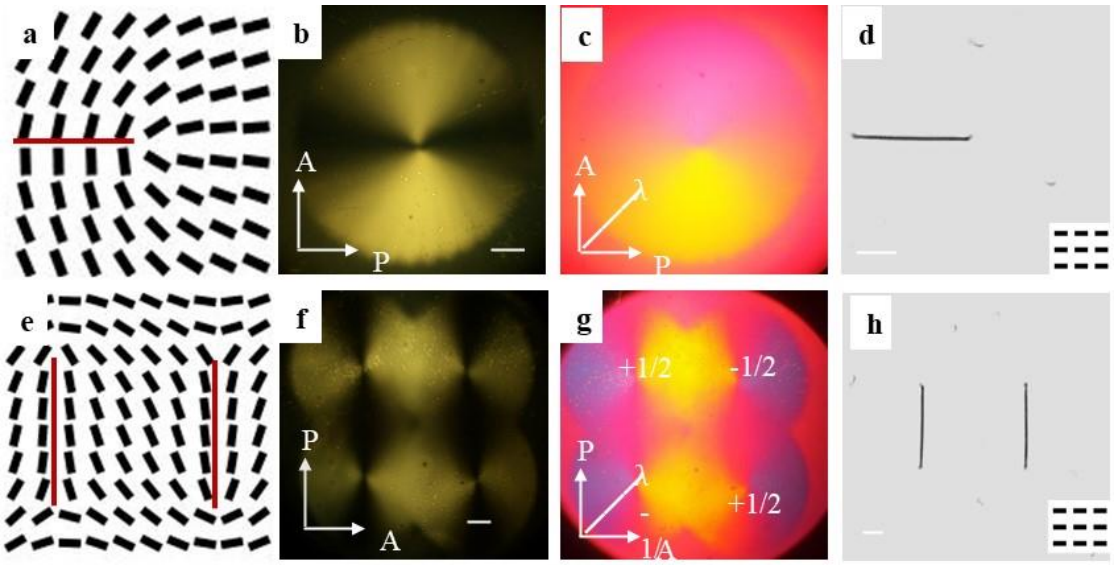

Figure 3.4 POM images of disclination lines using pattern with alternating +1/2 and -1/2 strengths

(**a**) Director field of the pattern with defect charge of +1/2; (**b**), (**c**) Polarizing microscopic image of this pattern without red plate and with red plate inserted, respectively; (**d**) Polarizing microscopic image of the disclination line formed in the assembled sample with patterned and uniform alignment substrates; (**e**) Director field of the pattern with alternating defect charge +1/2 and -1/2; (**f**), (**g**) Polarizing microscopic image of this pattern without red plate and with red plate inserted, respectively; (**h**) Polarizing microscopic image of the disclination line formed in the assembled sample with patterned and uniform alignment substrates; P and A represent the directions of polarizer and analyzer.

Different shapes and geometry, such as circular and square, of the disclinations lines are created and the self-assembly is achieved templated by those disclinations network. Not only the different shapes and geometry of the self-assembly can be achieved but also their reconfiguration is possible. It is demonstrated that disclinations network can be reconfigured and hence the amphiphiles also follow the dynamic changes and self-assemble in that template. When the orientation of the uniformly aligned molecules in the top substrate is changed by shining the linearly polarized light in the parallel direction, the disclinations network seems to contract. If we change the orientation of the uniform alignment by 90 degree, then it is realized that the circular lines contract by half the period and the amphiphilic assembly follows the network created by disclination lines, Fig. 3.5g-i.

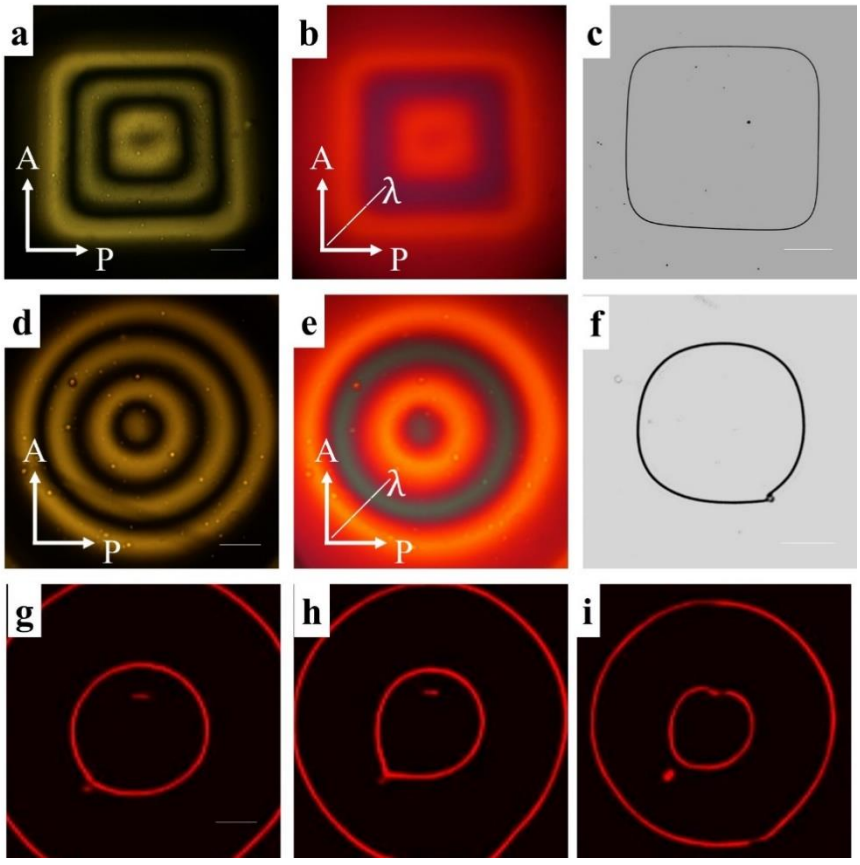

Figure 3.5 Self-assembly of molecules in different shapes and geometry

(**a**),(**d**) Polarizing micrographs of the square and circular pattern, respectively; (**b**), (**e**) Polarizing micrographs of the square and circular pattern with red plate inserted; (**c**), (**f**) Polarizing microscopic image of the square and circular disclination line network formed in the assembled sample with patterned and uniform alignment substrates; (**g**)-(**i**) Changes in the configuration of the self-assembly of the lipid molecules after shining the light through a linear polarizer; P and A represent polarizer and analyzer.

3.4 Results and Discussion

The simple pattern with strength circular +1 is created by using the simple formula M= R_1/R2, where R_1=R_2=1 in the parallel direction. After assembling this pattern with horizontally aligned uniform pattern, the incompatibility in the orientation of the LC molecules arises in the area marked with red lines which leads to the formation of the disclination lines followed by the self-assembly of the biomolecules. Since one substrate of the sample is aligned uniformly with azodye photoalignment layer, it entails the ability to reconfigure the molecular assembly by using light illumination, Fig 3.6. Fig. 1f shows that initial configuration of amphiphiles along x-axis with the uniform substrate aligned in x direction. When a linearly polarized light along x-axis is shone through the uniform azo-dye substrate, the azo-dye layer will be realigned perpendicularly to the linear polarization, i.e. y-axis, so that the defect line array would change the configuration from x-axis to y-axis and amphiphilic assemblies in the defect lines follow this reconfiguration, Fig. 3.6g-h. Note that the other patterned substrate is coated with a passivation layer of liquid crystalline polymer so it is not changed by the light illumination. Due to the reconfiguration of the disclination line network, the amphiphilic assemblies are transported following this dynamic motion, and the final amphiphilic assemblies are along y-axis, Fig. 3.6h. By simply using a linearly polarized light, the reconfigurations of the molecular assemblies are easily induced by programming the

defect lines template. The change of director field on the LC after shining the uniformly aligned substrate with linearly polarized light can be visualized by using simulation technique, Fig 3.6i-k.

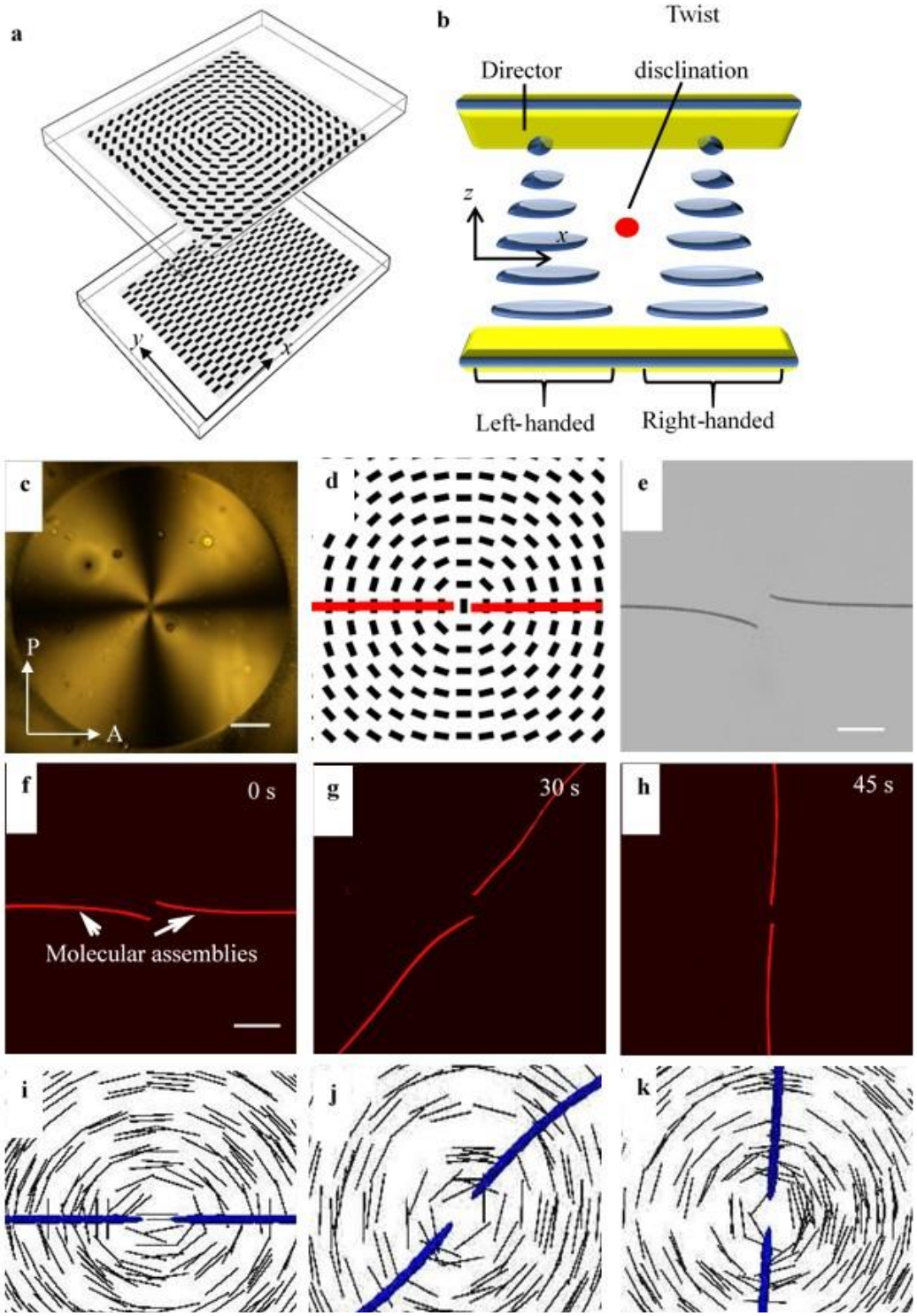

Figure 3.6 Templated molecular self-assembly by LC defect lines and their reconfiguration in a simple pattern by using light

(**a**) Schematic of assembling two substrates; One with topological orientation pattern and the other with uniform orientation along x-axis; **(b)** Schematic of how the Director field of the patterned substrate with circular +1 defect at the center; The red lines indicate the position of disclination lines; **(e)** Optical microscope image of formed disclinations lines; **(f)** Fluorescence microscope image of obtained BODIPY-labelled amphiphile assemblies; (**f**)-(**h**) Stepwise reconfiguration of the self-assembly of the molecules by shining light through linear polarizer on the uniformly aligned substrate at 0 sec (**f**), 30 sec (**g**), and 45 sec (**h**); (**i**)-(**k**) Schematic illustrations of how the director field changes accordingly; Scale bar is 200 μm.

Not only the simple patterns with singular defect but also the patterns with defect lines in array are created in order to explore the understanding of how will the self assembly of the lipid molecules be influenced if there are not one but multiple disclination lines as well as to realize the shape change of self assembly. So, for this effort, we generated the the pattern of strength +1 and -1 in an array by having R_1=1 and R_2=1 in the parallel and antiparallel directions, respectively, Fig. 3.7b. When the substrate with uniform alignment in horizontal direction is assembled with the patterened substrate of strength 1 array, the disclination lines are expected to be formed on the area marked with red line, Fig. 3.7a. In the similar manner, the self assembly of the biomolecules is followed on that path of disclinations network, Fig. 3.7d. But when the substrate with horizontal uniform alignment is shone a linearly polarized light in the parallel direction, the azo dye molecules will align perpendicularly to that direction and thus the position of the disclination lines network will change gradually from horizontal to vertical, Fig. 3.7d-h. The graph of Angle vs Time clearly depicts how the shape of the lines is changing with time. The schematic of the varying director field with respect to the external stimuli, i.e. light is portrayed in Fig. 3.7i-m.

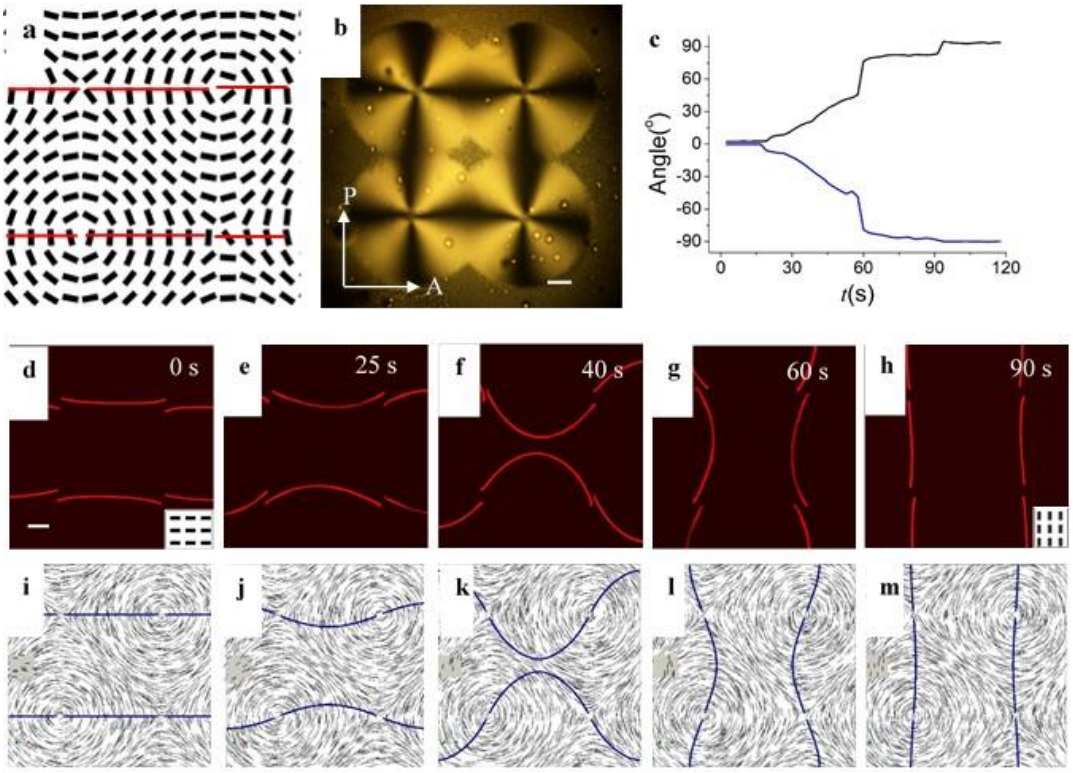

Figure 3.7 Predesigned self-assembly of amphiphiles in LC defect line array and their reconfiguration

Note that the substrate with uniform alignment along x-axis; **(a)** Director field of (+1, -1) defect array; The red lines indicate the position of disclination line array; **(b)** Optical microscope image of patterned substrate; **(c)** Graph showing how the geometry of the lines change with time due to the change in the orientation of the uniform alignment from horizontal to vertical direction; (**d**)-(**h**) Fluorescence microscope image of stepwise configuration of BODIPY-labelled amphiphile assemblies in the disclination line array at 0 sec (**d**), 25 sec (**e**), 40 sec (**f**), 60 sec (**g**), and 90 sec (**h**); (**i**)-**(m)** Schematic presentation of the dynamic change in the director field for respective configuration of the self-assembly; Scale bar is 200 μm.

To demonstrate an ability of pre-designing different configurations of amphiphilic assemblies and to realize the changes in geometry of the self-assembly by using the reconfiguration technique, more complex director fields are generated. A lattice of alternating +1/2 and -1/2 topological defects are designed with R_1=1 and R_2=2 in the parallel and antiparallel directions, respectively, Fig. 3.8b. After the assembly of horizontal uniform alignment with the patterned one, the

disclination lines are formed in the red line zone, which actually trigger the self-assembly of the amphiphiles, Fig. 3.8d. The geometry of the self-assembled lipid molecules will change when the uniform substrate is exposed to linearly polarized light in the parallel direction, Fig. 3.8d-h. It is clearly observable that there are two lines of assembly in the beginning and they change their geometry and become four lines of assembly at the end. How they change their shapes and geometry is portrayed by a graph of Angle vs Time, Fig. 3.8c. The lines are completely changing their geometry by a rotation of π, which might be fruitful in the biomedical application. The schematic of the change in the director field of the LC with change in the alignment of the azodye molecules due to the exposure of light is shown in Fig. 3.8i-m.

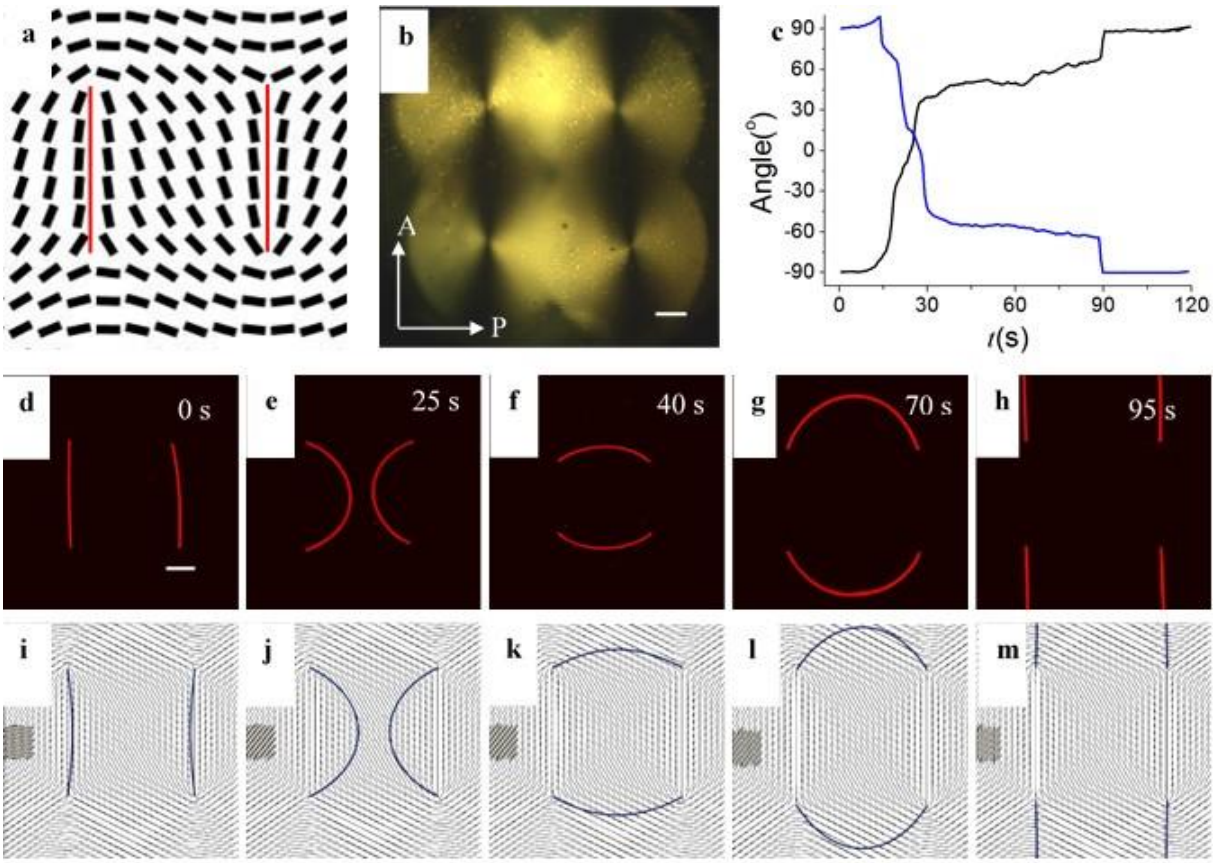

Figure 3.8 Reconfiguration of self-assembly to achieve the change in geometry

Note that the substrate with uniform alignment along x-axis; **(a)** Director field of strength (+1/2, -1/2) defect array; The red lines indicate the position of disclination line array; **(b)** Optical microscope image of patterned substrate; **(c)** Graph showing how the geometry of the lines change with time due to the change in the orientation of the uniform alignment from horizontal to vertical direction; (**d**)-(**h**) Fluorescence microscope image of stepwise configuration of BODIPY-labelled amphiphile assemblies in the disclination line array at 0 sec (**d**), 25 sec (**e**), 40 sec (**f**), 70 sec (**g**), and 95 sec (**h**); (**i**)-**(m)** Schematic presentation of the dynamic change in the director field for respective configuration of the self-assembly; Scale bar is $200\,\mu m$.

The application of the reconfiguration of self-assembly of the biomolecules isn't only limited to the position shifting and geometry change of the assembly. But to the farther extent, it entails the most crucial part in the biomedical application, which is shape change. The self-assembly of amphiphiles is also able to change their shape with a simple reconfiguration technique by using light. Fig. 3.9b-f show that the annihilation of the self-assembly of the lipid molecules when the vertically aligned uniform substrate was exposed to the linearly polarized light to make it horizontally aligned. Not only that, the amphiphiles assembly can also shift its position in 3D space as shown in fig. 3.9h-j. The linear graph of displacement vs time also clarifies that the lines are moving in the space after shining the linearly polarized light by changing its uniform alignment direction from vertical to horizontal. This might open so many opportunities in the medical physics, such as drug delivery and other cargo stuffs. The shape change is not limited to annihilation of the amphiphiles assembly, but we can also achieve a rectangular amphiphiles assembly from circular and vice-versa.

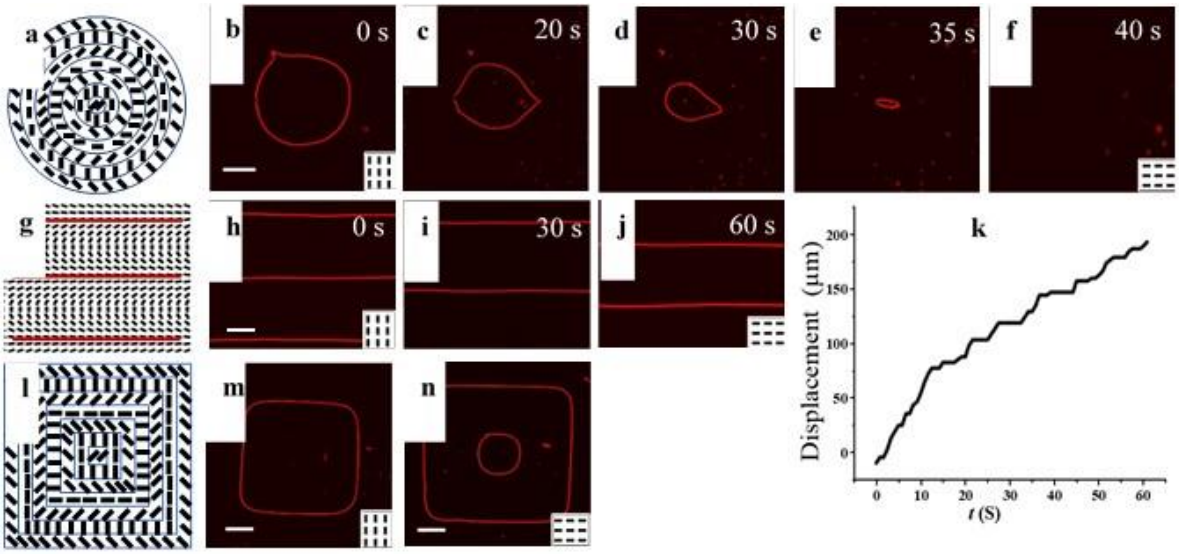

Figure 3.9 Reconfiguration of self-assembly of biomolecules to achieve the change in shape

(a) Director field of the pattern O; **(b)**-**(f)** Fluorescence micrographs of annihilation of the self assembly of lipids in the pattern 'O' due to the change in the orientation of the uniform alignment from vertical (**b**) to horizontal direction (**f**) as the top substrate is being exposed to the linearly polarized light; (**g**) Director field of the pattern 'C'; (**h**)-(**j**) Fluorescence micrograph of the stepwise configuration of the self assembly of the lipid molecules with different orintation of the uniform alignment from vertical to horizontal direction in consecutive times at 0 sec (**h**), at 30 sec (**i**), and at 60 sec (**j**); (**k**) Graph of displacement of the molecules with respect to time as the uniform alignment changes from vertical to horizontal direction; (**l**) Director field of the square pattern; (**j**)-(**k**) Fluorescence micrograph of the self assembly of the molecules when the orientation of the uniform alignment is vertical (**j**), and horizontal (**k**). Scale bar is 200 μm.

Chapter 4. Conclusions

To summarize, we propose an approach to design and create programmable molecular self-assembly structures in a deterministically predesigned manner. Various configurations, geometries and shapes of molecular assemblies are achieved by photopatterning the liquid crystalline media that amphiphiles are dispersed. This method is simple and can be fine-tuned to achieve any pre-designed molecular assembles and easily extended to any length scale. The arbitrary shapes of molecular assemblies are not limited to the current work and can be expanded to other different shapes due to versatility of designed patterns. Due to the sensitivity of liquid crystal to external stimuli, the created molecular assembly can be reconfigured by using light and mechanical shear. This programmability can also be achieved by other stimuli such as temperature, confinement, electric and magnetic fields. Such efforts are in progress. The resulting reconfigurable, programmable and predesigned molecular self-assembly opens opportunities for designing new dynamic functional bionanomaterials and developing new active soft materials for applications in nanoscience and nanomedicine.

References

1 Dierking, I. & Archer, P. Imaging liquid crystal defects. *RSC Advances* **3**, 26433-26437 (2013).

2 Whitesides, G. M. & Grzybowski, B. Self-assembly at all scales. *Science* **295**, 2418-2421, doi:DOI 10.1126/science.1070821 (2002).

3 Chakrabarty, R., Mukherjee, P. S. & Stang, P. J. Supramolecular Coordination: Self-Assembly of Finite Two- and Three-Dimensional Ensembles. *Chemical Reviews* **111**, 6810-6918, doi:10.1021/cr200077m (2011).

4 Zhao, X. *et al.* Molecular self-assembly and applications of designer peptide amphiphiles. *Chemical Society Reviews* **39**, 3480-3498, doi:10.1039/B915923C (2010).

5 Huck, W. T. *Nanoscale assembly: chemical techniques*. (Springer, 2005).

6 Poulin, P., Stark, H., Lubensky, T. C. & Weitz, D. A. Novel colloidal interactions in anisotropic fluids. *Science* **275**, 1770-1773 (1997).

7 Smalyukh, I. I., Lavrentovich, O. D., Kuzmin, A. N., Kachynski, A. V. & Prasad, P. N. Elasticity-Mediated Self-Organization and Colloidal Interactions of Solid Spheres with Tangential Anchoring in a Nematic Liquid Crystal. *Physical Review Letters* **95**, 157801 (2005).

8 Muševič, I., Škarabot, M., Tkalec, U., Ravnik, M. & Žumer, S. Two-Dimensional Nematic Colloidal Crystals Self-Assembled by Topological Defects. *Science* **313**, 954-958, doi:10.1126/science.1129660 (2006).

9 Ognysta, U. *et al.* 2D Interactions and Binary Crystals of Dipolar and Quadrupolar Nematic Colloids. *Physical Review Letters* **100**, 217803 (2008).

10 Wood, T. A., Lintuvuori, J. S., Schofield, A. B., Marenduzzo, D. & Poon, W. C. K. A Self-Quenched Defect Glass in a Colloid-Nematic Liquid Crystal Composite. *Science* **334**, 79-83, doi:10.1126/science.1209997 (2011).

11 Senyuk, B. I. *et al.* Topological colloids. *Nature* **493**, 200-205 (2013).

12 Mundoor, H., Senyuk, B. & Smalyukh, I. I. Triclinic nematic colloidal crystals from competing elastic and electrostatic interactions. *Science* **352**, 69-73, doi:10.1126/science.aaf0801 (2016).

13 Blanc, C., Coursault, D. & Lacaze, E. Ordering nano- and microparticles assemblies with liquid crystals. *Liquid Crystals Reviews* **1**, 83-109, doi:10.1080/21680396.2013.818515 (2013).

14 Pishnyak, O. P., Tang, S., Kelly, J. R., Shiyanovskii, S. V. & Lavrentovich, O. D. Levitation, lift, and bidirectional motion of colloidal particles in an electrically driven nematic liquid crystal. *Phys Rev Lett* **99**, 127802 (2007).

15 Luo, Y., Serra, F. & Stebe, K. J. Experimental realization of the "lock-and-key" mechanism in liquid crystals. *Soft Matter* **12**, 6027-6032, doi:10.1039/C6SM00401F (2016).

16 Lintuvuori, J. S. *et al.* Colloidal Templating at a Cholesteric-Oil Interface: Assembly Guided by an Array of Disclination Lines. *Physical Review Letters* **110**, 187801 (2013).

17 Foffano, G., Lintuvuori, J. S., Tiribocchi, A. & Marenduzzo, D. The dynamics of colloidal intrusions in liquid crystals: a simulation perspective. *Liquid Crystals Reviews* **2**, 1-27, doi:10.1080/21680396.2013.878672 (2014).

18 Voloschenko, D., Pishnyak, O. P., Shiyanovskii, S. V. & Lavrentovich, O. D. Effect of director distortions on morphologies of phase separation in liquid crystals. *Physical Review E* **65**, 060701 (2002).

19 Yoon, D. K. *et al.* Internal structure visualization and lithographic use of periodic toroidal holes in liquid crystals. *Nat Mater* **6**, 866-870 (2007).

20 Pires, D., Fleury, J. B. & Galerne, Y. Colloid particles in the interaction field of a disclination line in a nematic phase. *Phys Rev Lett* **98**, 247801, doi:Artn 247801 Doi 10.1103/Physrevlett.98.247801 (2007).

21 Yoshida, H., Asakura, K., Fukuda, J. & Ozaki, M. Three-dimensional positioning and control of colloidal objects utilizing engineered liquid crystalline defect networks. *Nature Communications* **6**, 7180, doi:10.1038/ncomms8180 (2015).

22 Wang, X., Miller, D. S., Bukusoglu, E., de Pablo, J. J. & Abbott, N. L. Topological defects in liquid crystals as templates for molecular self-assembly. *Nat Mater* **15**, 106–112, doi:10.1038/nmat4421 (2016).

23 Wang, X., Miller, D. S., Bukusoglu, E., de Pablo, J. J. & Abbott, N. L. Topological defects in liquid crystals as templates for molecular self-assembly. *Nat Mater* **15**, 106, doi:10.1038/nmat4421 (2016).

24 Peng, C., Turiv, T., Guo, Y., Wei, Q.-H. & Lavrentovich, O. D. Command of active matter by topological defects and patterns. *Science* **354**, 882-885, doi:10.1126/science.aah6936 (2016).

25 Guo, Y. *et al.* High-Resolution and High-Throughput Plasmonic Photopatterning of Complex Molecular Orientations in Liquid Crystals. *Advanced Materials* **28**, 2353–2358, doi:10.1002/adma.201506002 (2016).
26 Peng, C. *et al.* Liquid crystals with patterned molecular orientation as an electrolytic active medium. *Physical Review E* **92**, 052502 (2015).
27 de Gennes, P. G. & Prost, J. *The Physics of Liquid Crystals*. (Clarendon, Oxford, 1993).
28 Kleman, M. & Lavrentovich, O. D. *Soft matter physics: an introduction*. (Springer-Verlag New York, Inc. , 2003).
29 Wang, M., Li, Y. & Yokoyama, H. Artificial web of disclination lines in nematic liquid crystals. *Nature communications* **8**, 1-7 (2017).
30 Harkai, S., Murray, B. S., Rosenblatt, C. & Kralj, S. Electric field driven reconfigurable multistable topological defect patterns. *Physical Review Research* **2**, 013176 (2020).
31 Duclos, G. *et al.* Topological structure and dynamics of three-dimensional active nematics. *Science* **367**, 1120-1124 (2020).